



ESTONIAN UNIVERSITY OF LIFE SCIENCES
Institute of Forestry and Engineering

Richard Erelt

**ASSESSMENT OF NANOPARTICLES-BASED ADDITIVES
IN JET-FUELS COMBUSTION**

NANOOSAKESTEL PÕHINEVATE LISANDITE MÕJU
HINNANG REAKTIIVKÜTUSTE PÕLETAMISEL

Master's thesis
Energy Application Engineering

Supervisor: Prof. Erwan Rauwel, *PhD; DSc*
Co-supervisor: Dr. Siim Küünal, *PhD*
Co-supervisor: Mr. Karl-Erik Unt, *MSc*

Tartu 2024

Eesti Maaülikool Kreutzwaldi 1, Tartu 51014		Magistritöö lühikokkuvõte	
Autor: Richard Ereht		Õppekava: Energiakasutus	
Pealkiri: Nanoosakestel põhinevate lisandite mõju hinnang reaktiivkütuste põletamisel			
Lehekülgi: 72	Jooniseid: 30	Tabeleid: 5	Lisasid: 1
Osakond / Õppetool: Energiakasutuse õppetool ETIS-e teadusvaldkond ja CERC S-i kood: T150 Materjalitehnoloogia; T140 Energeetika Juhendaja(d): Erwan Yann Rauwel, <i>PhD</i> ; Siim Küünal, <i>PhD</i> ; Karl-Eerik Unt, <i>MSc</i> Kaitsmiskoht ja -aasta: Metsanduse ja inseneeria instituut 2024			
<p>Maailm on liikumas fossiilkütustelt elektrile nii transpordis kui ka muudes sektorites, et saavutada jätkusuutlikkus ja vähendada süsinikdioksiidi heitkoguseid. Reaktiivkütus on lennunduse jaoks endiselt ülioluline oma suure energiatiheduse ja elektriliste alternatiivide puudumise tõttu pikamaalendudeks. Nanoosakeste lisamine lennukikütusele on paljulubav viis heitkoguste vähendamiseks, suurendades põlemistõhusust, vähendades õhustranspordi süsiniku jalajälge ja vähendades kahjulike heitgaaside eraldumist.</p> <p>Lõputöös viidi läbi viis sünteesi, kasutades rohesünteesi lähenemisviisi. Päevalilleseemneid kasutati nende kõrge õlisisalduse tõttu prekursorina, mis hõlbustas nanoosakeste homogeenset hajumist lennukikütuses. Jet A-1 ja Jet A-1 nanokütustega viidi läbi füüsikalised ja keemilised testid, sealhulgas destilleerimisekarakteristikud, leekpunkti ja tiheduse analüüsi. Seejärel viidi läbi mootorikatsed, et mõõta erinevaid tööparameetreid, nagu õhukiirus, temperatuur, rõhk ja heitgaaside koostis. Tulemused näitasid, et ZnO nanoosakestega on paranenud mootori jõudlusnäitajad, sealhulgas suurenenud õhukiirused, temperatuurid ja rõhud. Nanoosakeste lisamisega kaasnes aga suurem CO, CO₂, süsivesinike ja NO_x heitkogus, mis võis tuleneda sünteesist. Need leiud on vastuolus kirjandusega, rõhutades vajadust täiendavate uuringute järele, et mõista nanoosakeste kaasamise erinevaid mõjusid mootori erinevates konfiguratsioonides ja töötingimustes. Tulevased uuringud peaksid keskenduma nanoosakeste sünteesi, stabiilsuse ja kontsentratsiooni optimeerimise täiustamisele, lisaks uurima nende pikaajalist mõju kütusefiltritele ja heitkoguste vähendamise strateegiatele.</p>			
Märksõnad: Tsinkoksiid, nanoosakesed, Jet A-1, kütuselisand, õhustransport			

Estonian University of Life Sciences Kreutzwaldi 1, Tartu 51014		Abstract of Master's Thesis	
Author: Richard Ereht		Curriculum: Energy Application Engineering	
Title: Assessment of Nanoparticles-Based Additives in Jet-Fuels Combustion			
Pages: 72	Figures: 30	Tables: 5	Appendixes: 1
Department / Chair: Chair of Energy Application Engineering Field of research and (CERC S) code: T150 Material technology; T140 Energy research Supervisors: Erwan Yann Rauwel, <i>PhD</i> ; Siim Küünal, <i>PhD</i> ; Karl-Eerik Unt, <i>MSc</i> Place and date: Institute of Forestry and Engineering 2024			
<p>The world is shifting from fossil fuels to electricity to reduce carbon emissions, but jet fuel remains essential for aviation due to its high energy density and lack of viable electric alternatives for long flights. Adding nanoparticles to jet fuel offers a promising way to reduce emissions by enhancing combustion efficiency, decreasing carbon footprint of air freight, and reducing the release of harmful exhaust gases.</p> <p>In this study, five syntheses were performed using a green synthesis approach, with sunflower seeds used as a precursor due to their high oil content, facilitating homogeneous dispersion of nanoparticles within the jet fuel. Physical and chemical tests were performed on the Jet A-1 and Jet A-1 nanofuel, including distillation characteristics, flash point, and density analysis. Engine tests were then conducted to measure various parameters such as airspeed, temperature, pressure, and exhaust emissions. The results showed improved engine performance metrics with ZnO nanoparticles, including increased airspeeds, temperatures, and pressures. However, this enhancement was accompanied by slightly higher emissions of CO, CO₂, hydrocarbons, and NO_x that could originate from the way of synthesis itself. These findings contrasted with literature, highlighting the need for further research to understand the varying effects of nanoparticle incorporation in different engine configurations and operating conditions. Future research should focus on improving nanoparticle synthesis, stability, and concentration optimization, alongside investigating their long-term effects on fuel filters and emissions reduction strategies.</p>			
Keywords: Zinc oxide, nanoparticles, Jet A-1, fuel additive, air freight			

TABLE OF CONTENTS

LIST OF ABBREVIATIONS.....	5
INTRODUCTION.....	6
1. NANOPARTICLES AS FUEL ADDITIVES.....	8
1.1. Operating principle of gas turbines and fuel properties.....	8
1.2. Commonly tested nanoparticles as fuel additives.....	10
1.3. Concentration of nanoparticles.....	11
1.3.1. Aluminium oxide.....	12
1.3.2. Zinc oxide.....	14
1.4. Nanoparticles in jet fuel.....	15
1.5. Nanoparticle manufacturing.....	18
1.5.1. Top-down method for producing nanoparticles.....	19
1.5.2. Bottom-up method for producing nanoparticles.....	20
1.5.3. Green synthesis.....	21
1.6. Safety, risks, and drawbacks of using nanoparticles as fuel additives.....	22
2. MATERIALS AND METHODOLOGY.....	25
2.1. Used laboratory equipment and software.....	25
2.2. Preparation of nanoparticles.....	31
2.2.2. Synthesis of Al ₂ O ₃ and ZnO nanoparticles.....	31
2.2.3. UV-vis spectrophotometer analyses.....	35
2.2.4. Heating plate temperature calibration.....	36
2.2.5. Preparation of fuel samples for analyses and engine tests.....	36
2.2.6. FTIR analyses.....	37
2.2.7. SEM analyses.....	37
2.2.8. XRD analyses.....	38
2.3. Engine tests.....	38
3. RESULTS AND DISCUSSION.....	39
3.1. Results of the preparation of the Nanoparticles.....	39
3.1.1. Results of the Al ₂ O ₃ and ZnO nanoparticles syntheses.....	39
3.1.2. Results of UV-vis spectrophotometer analyses.....	49
3.1.3. Temperature calibration of the heating plate temperature.....	53
3.1.4. FTIR analyses results.....	54
3.1.5. SEM analyses results.....	56
3.1.6. XRD analyses results.....	57
3.1.7. Fuel analyses results.....	58
3.2. Engine tests results.....	60
SUMMARY AND CONCLUSION.....	63
LITERATURE.....	65
ÜLDKOKKUVÕTE.....	69
APPENDIXES.....	71
Appendix A. Lihtlitsents lõputöö salvestamiseks ja üldsusele kättesaadavaks tegemiseks ning juhendajate kinnitus lõputöö kaitsmisele lubamise kohta.....	72

LIST OF ABBREVIATIONS

Ag ₂ O	– silver oxide
Al	– aluminium
Al ₂ O ₃	– aluminium oxide
APU	– auxiliary power unit
ATF	– aviation turbine fuel
B	– boron
BSFC	– brake-specific fuel consumption
BTE	– brake thermal efficiency
CeO ₂	– cerium oxide
CNT	– carbon nanotubes
CO	– carbon monoxide
CuO	– copper oxide
DPF	– diesel particulate filters
EDS	– energy-dispersive X-ray spectroscopy
EGR	– exhaust gas recirculation
Fe	– iron
Fe ₂ O ₃	– iron oxide
FTIR	– Fourier-transform infrared spectroscopy
GHG	– greenhouse gas
GOME	– grapeseed oil methyl ester
HC	– hydrocarbons
HVO	– hydrotreated vegetable oil
LASiS	– laser ablation synthesis in solution
Mg	– magnesium
MgO	– magnesium oxide
MWCNT	– multiwall carbon nanotubes
NAFs	– nano-additive fuels
NO _x	– nitric oxide and nitrogen dioxide
ppm	– parts-per-million
SAF	– sustainable aviation fuel
SCR	– selective catalytic reductions
SEM	– scanning electron microscope
SFC	– specific fuel consumption
TiO ₂	– titanium oxide
wt%	– weight percentage
XRD	– X-ray diffraction
ZnO	– zinc oxide
λ	– air-fuel equivalence ratio

INTRODUCTION

The world is now moving from fossil fuels to electricity for many transportation and energy needs, driven by the pursuit of sustainability and reduced carbon emissions. However, despite these advances, jet fuel remains essential for aviation due to its high energy density and the current lack of viable electric alternatives for powering aircraft over long distances. In addition, biofuel does not yet meet the required quality to be used in plane engines. One promising approach to reducing emissions from jet fuel is the addition of nanoparticles, which could enhance combustion efficiency and decrease the production of harmful exhaust gases.

During the last decade, there has been a lot of research done about the use of nanoparticles as fuel additives in internal combustion engines. The fuel additives are usually chemicals that are added to the fuel to improve engine performance or add properties that are not specific to the base fuel. The main goal of fuel additives is the reduction of fuel consumption and harmful exhaust gasses but also improvement in engine power and torque. Due to their size, nanoparticle fuel additives can dramatically change combustion characteristics. Many researchers have shown that nanoparticle additives improve both fuel efficiency and reduce exhaust emissions. [2], [3], [4]

The objective of the present work is to test the effectiveness of nanoparticles as fuel additives in jet fuel for performance improvement and reduction in harmful emissions such as hydrocarbons (HC), carbon monoxide (CO), and smoke.

The main goal of this master's thesis is to:

- provide an overview of nanoparticles, including their production and applications;
- review research on using nanoparticles in fuel;
- synthesise nanoparticles;
- prepare and analyse Jet A-1 fuel mixed with nanoparticle additives;
- test jet turbine engines with both standard Jet A-1 fuel and Jet A-1 fuel with nanoparticle additives;
- analyse and evaluate test results to determine the suitability of nanoparticle additives in Jet A-1 fuel.

The author's selection of this topic is motivated by their background in chemistry and biology, as well as their current focus on energy application engineering. Chemistry is crucial for understanding the synthesis, properties, and interaction of these additives with

fuel molecules and combustion processes. Biology comes into play when considering the potential toxicological effects on organisms and the environment. The integration of nanoparticle additives in fuel requires a multidisciplinary approach, combining knowledge from chemistry, biology, and engineering to optimize fuel performance, reduce emissions, and address any potential adverse impacts.

The first chapter addresses nanoparticles and their diverse applications, including their integration into fuel compositions. Within this chapter, an overview of nanoparticle synthesis methodologies is provided. The second chapter details the materials and methods employed for the green synthesis of Al_2O_3 and ZnO nanoparticles, along with subsequent characterization and testing protocols. In the concluding third chapter, a detailed discussion is provided on the synthesis outcomes and testing results, including analyses of fuel compositions and evaluations of engine performance.

The author expresses gratitude to Prof. Erwan Rauwel, Dr. Siim Küünal, and Karl-Eerik Unt for their valuable knowledge, guidance, and support throughout the thesis writing process. Financial support from Thematic research and development programs (TEM-TA144) is acknowledged. The author extends thanks to the Estonian Aviation Academy Department of Aeronautical Engineering for providing the jet turbine engine for testing purposes.

1. NANOPARTICLES AS FUEL ADDITIVES

Integrating nanoparticle additive fuels presents a promising avenue for curbing greenhouse gas (GHG) emissions from airplanes. By leveraging nanoparticles that possess high surface area-to-volume ratios and tailored properties, fuel combustion efficiency can be significantly enhanced. These additives facilitate more complete combustion, resulting in reduced emissions of carbon dioxide (CO₂), nitrogen oxides (NO_x), and other pollutants. Implementing nanoparticle additive fuels thus represents a crucial step towards achieving greener aviation, fostering environmental sustainability while maintaining the efficiency and reliability of air travel.

1.1. Operating principle of gas turbines and fuel properties

Similar to diesel or gasoline engines, a gas turbine is a form of internal combustion engine that functions through the intake, compression, combustion, and exhaust cycle. However, a significant distinction lies in the fundamental motion: while a reciprocating engine moves back and forth, a gas turbine operates with rotary motion. [1]

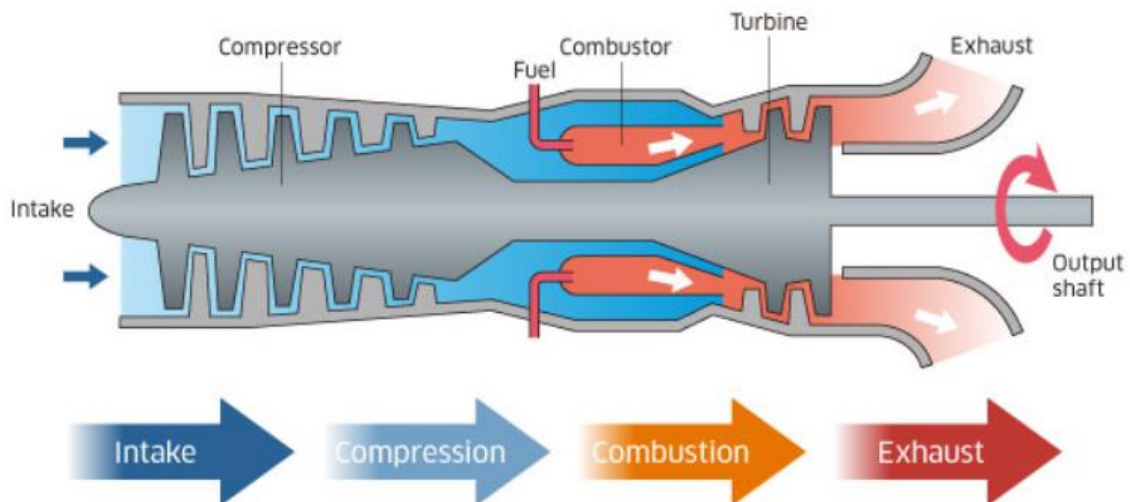


Figure 1.1. Operating principle of a gas turbine engine. [1]

The fundamental concept of a gas turbine involves several key steps (figure 1.1). Initially, air undergoes compression by a compressor, and the compressed air is directed into the combustor. Within the combustor, fuel undergoes continuous combustion, generating gas at elevated temperatures and pressures. This gas is then expanded within the turbine, which consists of a vaned rotor constructed by affixing numerous blades to a circular disk. This expansion results in the generation of rotational energy, which in turn powers the compressor in the earlier stage. The remaining energy is transferred through an output shaft. [1]

Fuel properties encompass a spectrum of characteristics essential for understanding fuel behaviour and its impact on engine performance and safety. When dealing with nano additive fuels, several key parameters are considered. [2]

Density, representing the mass of fuel per unit volume, influences energy storage capacity and can alter fuel efficiency and combustion dynamics. Higher-density fuels contain more energy per unit volume, which can impact factors such as fuel efficiency and combustion characteristics. [2]

Viscosity measures a fluid's resistance to flow. In fuels, viscosity influences how easily the fuel can flow through fuel lines and injectors in an engine. Higher viscosity fuels may be more difficult to atomize and combust efficiently, potentially affecting engine performance and emissions. [2]

The flash point indicates the temperature at which fuel vapours can ignite when exposed to an ignition source, while the fire point signifies the temperature at which the fuel's vapor sustains combustion. In terms of combustion, higher flash point and fire point of the fuel are generally considered less favourable. A higher flash point indicates that the fuel is less volatile and may require higher temperatures to vaporize and ignite, potentially leading to incomplete combustion and reduced engine efficiency. Similarly, a higher fire point suggests that the fuel is more resistant to sustained combustion once ignited, which can hinder the combustion process and result in inefficient energy release. Therefore, lower flash point and fire point fuels are typically preferred for better combustion efficiency and engine performance. [2]

Calorific value denotes the amount of heat released per unit mass of fuel burned, directly impacting engine power output and fuel efficiency. Higher calorific values indicate greater energy production from combustion. [2]

Ignition delay, also known as delay time, refers to the time between fuel injection and combustion initiation in a diesel engine. Shorter delays result in more efficient combustion processes, leading to improved engine performance and reduced emissions. [2]

The cetane number measures diesel fuel's combustion speed and ignition requirements, indicating faster combustion with higher numbers. Engines with higher speeds operate more efficiently with fuels possessing higher cetane numbers. [2]

Fuel thermal conductivity affects combustion by determining how efficiently heat is transferred within the combustion chamber. Higher thermal conductivity promotes uniform heating and vaporization of the fuel, leading to improved combustion efficiency and engine performance. However, excessively high thermal conductivity may lead to challenges such as incomplete combustion or ignition difficulties. Therefore, optimizing thermal conductivity is essential for efficient combustion. [2]

Brake-specific fuel consumption (BSFC) and specific fuel consumption (SFC) are metrics used to evaluate engine fuel efficiency. SFC measures the amount of fuel consumed per unit of power output, providing a general indicator of fuel efficiency. In contrast, BSFC refines this measure by considering only the useful power output of the engine relative to its brake horsepower, excluding losses from accessories like the alternator. [2]

Cylinder pressure, influenced by fuel properties, combustion efficiency, and engine design, directly impacts engine performance. Increased pressure leads to greater force exerted on the piston, resulting in enhanced power output and torque. Optimization of fuel properties and combustion processes to achieve ideal cylinder pressure and ignition delay is crucial for maximizing engine efficiency, and performance, and minimizing emissions. [2]

1.2. Commonly tested nanoparticles as fuel additives

The fuel additives can improve the combustion properties of the fuel, reduce harmful emissions, improve stability and handling of fuel, provide engine cleanliness, ensure protection from corrosion, and increase fuel economy. Fuel additives at least one dimension less than 100 nm are considered nanosized fuel additives. Nano-fuel is a two-phase colloidal mixture consisting of nano-sized particles dispersing in a base fuel. [2]

Nanoparticle fuel additives have been tested on a variety of fuels or fuel mixtures such as diesel, diesel-biodiesel, gasoline, kerosene, JP-10, and solid propellants. These fuels were

altered by additions of metallic non-metallic nanoparticles, or carbon-based nanomaterials such as aluminium (Al), iron (Fe), boron (B), magnesium (Mg), copper oxide (CuO), magnesium oxide (MgO), silver oxide (Ag₂O), iron oxide (Fe₂O₃), aluminium oxide (Al₂O₃), zinc oxide (ZnO), titanium oxide (TiO₂), cerium oxide (CeO₂), carbon nanotubes (CNT), multiwall carbon nanotubes (MWCNT)... [2], [3], [4]

Studies have shown that the appropriate concentration of nanoparticles promotes the evaporation of fuel droplets, however, the excess concentration can reduce the evaporation rate [2]. Due to their nanosize, the large surface-to-volume ratio of nanoparticles make combustion more efficient by lowering the thermal decomposition temperature of solid fuels and ensuring the continuity of combustion reactions [3]. In addition, they provide rich air-fuel mixtures by improving the atomization mechanism in liquid fuels [3].

Nano-additive fuels (NAFs) have potential advantages such as higher energy release, shortened ignition delay, and higher ignition probability [2], [3]. However, these benefits are limited in practice due to the formation of porous and dense residual particle aggregates, that contain incompletely burned nanoparticles [3]. In addition, nanoparticles can cause pre-ignition, meaning that the air-fuel mixture in the cylinder will ignite before the spark plug fires [3].

Metallic nanoparticles are commonly tested as fuel additives due to their high energy density and reactivity. Also, the nanometric size of additives provides a larger surface reaction area for fast oxidation. Several metals, such as aluminium, magnesium, boron, and zirconium, have superior volumetric energy densities than fossil fuels while being burned in the air. In addition, nanosized metal (Al, Fe) or metal oxides (Al₂O₃, Fe₂O₃) can also act as lubricants by providing rolling action and thereby reducing engine wear. [2]

1.3. Concentration of nanoparticles

The addition of nanoparticles to improve performance and reduce exhaust emissions can be beneficial, but excessive nanoparticle concentration can have negative effects. Too high nanoparticle concentrations can impact fuel properties like viscosity, density, flash point, fire point, calorific value, and cetane number. Increasing nanoparticle concentration leads to higher fuel density, flash point, and fire point. However, surpassing a critical limit of nanoparticle addition can result in issues such as increased pre-ignition and combustion

instability. These problems are primarily attributed to too high viscosity, lower calorific value, lower cetane number, and elevated flash point and fire point caused by exceeding the nanoparticle concentration threshold. [2]

To enhance the performance of fuel blends, it is necessary to add the minimum concentration of nanoparticle additives that will enable the improvement of the fuel characteristics and combustion without any additional drawbacks. Research indicates that this minimum concentration varies depending on the specific fuel and the type of nanoparticles employed. Typically, this critical concentration falls within the range of 20 to 30 ppm (20 to 30 mg/L). In an experiment, MgO nanoparticles were incorporated into a diesel-biodiesel blend within the range of 20 to 50 ppm. The study revealed that a concentration of 30 ppm of nanoparticles had only a slight impact on the fuel blend's properties, resulting in enhanced performance and reduced emissions compared to other concentrations. While 20 ppm of nanoparticles did not affect the performance. [2]

Typically, the upper limit of concentration that enhances the combustion performance of fuel during the primary atomization stage, leading to reduced droplet size and increased penetration, is 2 weight percentage (wt%) of nanoparticles. Once the concentration surpasses this threshold, both combustion performance and secondary atomization suffer due to a decline in evaporation rate. This decline is attributed to particle aggregation on the surface of NAF droplets during combustion. Although the fuel's thermal conductivity may elevate, the diffusion of fuel vapor from the droplet surface toward the combustion centre becomes increasingly challenging. Consequently, destructive micro explosions ensue as the crust formed by particle agglomerates thickens, leading to deviations from the d^2 -law. In the case of Al nanoparticles, the ideal concentration for improving fuel evaporation behaviour is 2.5 wt%. However, dilute concentrations below this value can cause significant improvements in combustion behaviour. [3]

1.3.1. Aluminium oxide

There has been research done on the addition of aluminium oxide nanoparticles in various concentrations to diesel and diesel blend fuels. Concentrations including 10, 15, 20, 30, 40, 50, 60, 100, and 150 ppm have been tested. [2], [3], [4]

The best improvement in combustion properties, lowest particle matter (PM) concentration, and gas emissions across different engine loads was observed with 100 ppm of Al_2O_3 nanoparticles. In one study, the addition of 100 ppm Al_2O_3 nanoparticles increased cylinder pressure and heat release rate by 6% and 13% respectively, compared to the fuel mixture without Al_2O_3 . Moreover, it resulted in a 4.7% increase in brake thermal efficiency and a 7.3% decrease in BSFC. Notably, CO, HC, nitric oxide, and NO_x emissions were reduced by 42.71%, 37.46%, and 12.37% respectively. Long-term exposure to these pollutants can cause neurological, reproductive, and respiratory effects, which can result in a variety of different types of cancer. [3]

However, some researchers suggest that lower concentrations of Al_2O_3 can yield better outcomes. In a study using lemongrass oil biodiesel with varying Al_2O_3 concentrations (10, 20, and 30 ppm), the optimal engine combustion performance and exhaust emissions were achieved with 20 ppm. This concentration led to a significant improvement of 11.5% in brake thermal efficiency (BTE), along with reductions of 40%, 6%, 31%, and 39% in HC, CO, NO_x , and smoke emissions respectively, compared to regular biodiesel. [4]

Similarly, another study investigated 20, 40, and 60 ppm concentrations of Al_2O_3 in Honge oil methyl ester biodiesel. It was found that the 40 ppm concentration exhibited superior engine combustion performance compared to both 20 and 60 ppm. This concentration resulted in a 10.57% increase in BTE and an 11.65% reduction in BSFC. Furthermore, HC, CO, and smoke emissions were reduced by 26.72%, 48.43%, and 22.84% respectively, while NO_x emissions increased by 11.27%. Higher NO_x levels are not desired since long-term exposure can cause respiratory diseases. [4]

The incorporation of Al_2O_3 nanoparticles into the fuel blend results in an increase in density, calorific value, and viscosity. In a particular study, the addition of 150 ppm of Al_2O_3 nanoparticles elevated the cetane number from 51.6 to 54.3. Moreover, higher concentrations of nanoparticles were found to reduce the delay period. [4]

Findings suggest that the size of particles plays a crucial role in ignition and combustion [4]. Smaller particle sizes demonstrated a higher level of reaction intensity [4]. The addition of nanoparticles in fuel showed an enhancement of combustion characteristics through the high surface-to-volume ratio exhibited by these nanoparticles [4]. A high surface-to-volume ratio promotes better air-fuel mixing during the combustion process [4]. It shows that smaller nanoparticles will be more efficient due to their larger active surface available to interact with the fuel during the combustion process [4]. Nanoparticles with sizes above 400 nm did

not exhibit a notable impact on primary atomization [3]. Primary atomization is an instance of intricate gas-liquid flow: in proximity to the nozzle, the liquid, initially delivered as a continuous jet, breaks down into filaments and droplets through interaction with the gas [3]. Moreover, in all experiments, the ignition probability of NAFs containing Al and Al₂O₃ nanoparticles was significantly higher compared to pure diesel [3].

1.3.2. Zinc oxide

In 2021, a master's thesis conducted at the Engine Laboratory of the Estonian University of Life Sciences examined the effects of 10 ppm of ZnO nanoparticles in diesel fuel under various engine loads (20%, 40%, 50%, 75%, and 100%). The results indicated that the addition of 10 ppm of ZnO nanoparticles did not significantly impact lambda (air-fuel equivalence ratio where $\lambda = 1.0$ is at stoichiometry, $\lambda < 1.0$ is a rich mixture, and $\lambda > 1.0$ is a lean mixture) and the amount of CO, CO₂, and soot produced. However, it was observed that the inclusion of 10 ppm of ZnO nanoparticles reduced hydrocarbon and NO_x exhaust gas values, which is important for the decrease of toxic exhaust by-product release. The power, torque, and engine efficiency trend lines remained similar to the control measurements. Based on these findings, future research was suggested to explore the addition of larger quantities of ZnO nanoparticles in the fuel, ranging from 20 to 40 ppm. [5]

In a separate study, the performance and emission characteristics of diesel-based nanofluids containing 50 ppm and 100 ppm of ZnO nanoparticles were investigated. The results showed an increase in BTE values and a decrease in BSFC compared to diesel fuel without nanoparticles. Additionally, as engine load and nanoparticle concentration increased, there was a reduction in NO_x, CO, and HC emissions. [3]

Other researchers explored the impact of ZnO nanoparticles in grapeseed oil methyl ester (GOME) biodiesel. The inclusion of ZnO nanoparticles increased BTE from 28.17% to 29.3% and decreased BSFC from 0.3258 kg/kWh to 0.3128 kg/kWh. Furthermore, reductions in NO_x, HC, and CO emissions were observed. Another study investigated the effects of different sizes of ZnO nanoparticles in mango seed biodiesel and found that blending biodiesel with 40 nm ZnO nanoparticles resulted in higher calorific value, cetane value, and improved combustion performance. [4]

In a different study, the physicochemical properties of fuels; diesel with 30 ppm ZnO nanoparticles, 20% Mahua biodiesel, and 20% Mahua biodiesel with 30 ppm ZnO nanoparticles were examined using a modified common rail direct injection engine (CRDI) (figure 1.2). In CRDI systems, fuel is directly injected into the cylinders of a diesel engine through a shared line known as the common rail, which links to all the fuel injectors. The engine test results demonstrated an overall enhancement of CRDI engine characteristics when 30 ppm of ZnO nanoparticles were added to diesel, with diethyl ether, and in Mahua biodiesel. [6]

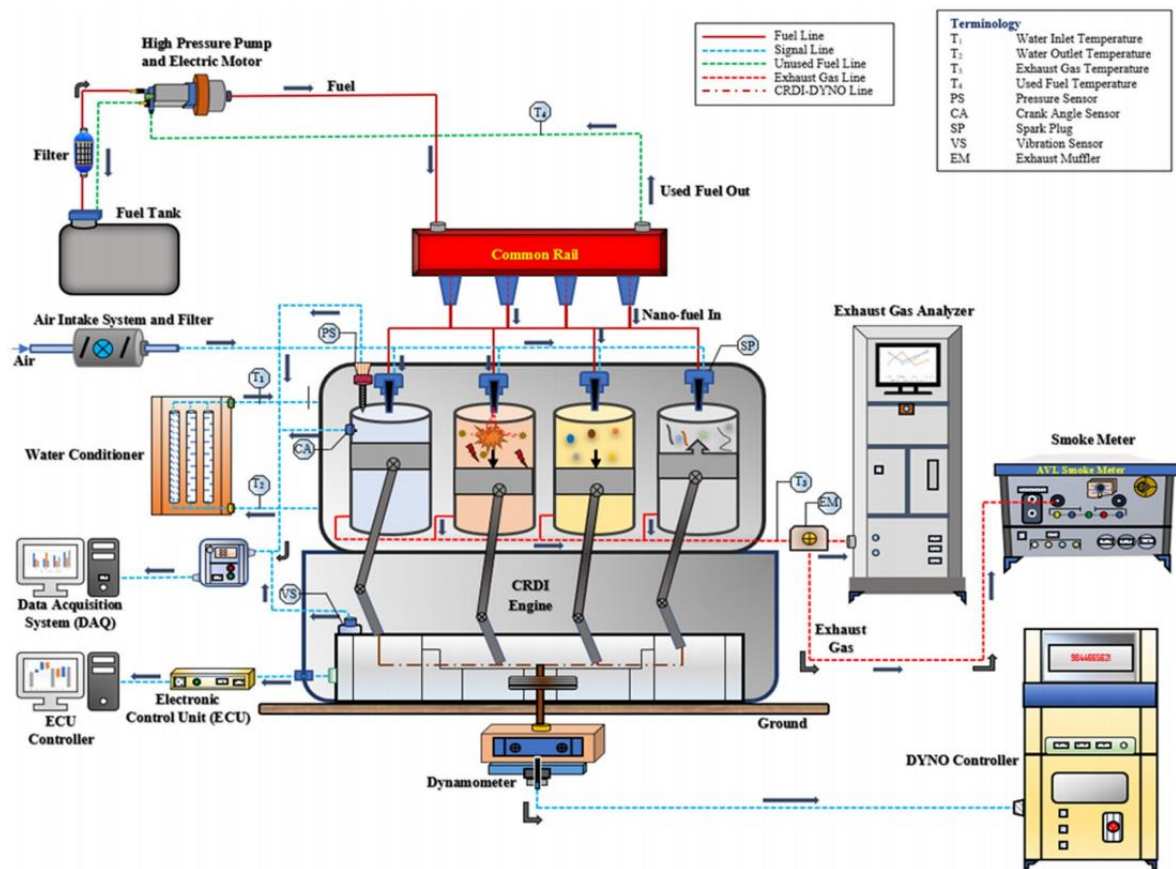


Figure 1.2. Schematic layout of computerized CRDI test engine. [6]

1.4. Nanoparticles in jet fuel

The emergence of sustainable aviation fuels (SAF) is seen as a promising method for reducing CO₂ emissions in the aviation sector in the near to mid-term, utilizing the current global fleet. Nonetheless, integrating SAF presents a significant challenge: to ensure

compatibility with existing and future civil aircraft fleets, any new 'drop-in' jet fuel, like SAF, must adhere to strict fuel specifications akin to conventional fossil-based fuels. Moreover, it's imperative for these fuels to be mixable with conventional counterparts, exhibit comparable behaviour, meet global standards, and uphold operational safety requirements. Nanoparticle additives are being explored as potential solutions to render SAF suitable for use in current and future civil aircraft fleets.

Nanoparticles have also been tested in jet fuels. Jet A is being used in the United States and Jet A-1 is the predominant choice in most other parts of the world, primarily differing in freezing points. Jet A-1 and diesel are both hydrocarbon fuels, but they have different compositions and uses. Jet A-1 is specialized for aviation, with low sulphur content and specific density for jet engines. Diesel, used in various vehicles and industries, has varying sulphur content and density. Jet A-1 has higher flash and fire points for aviation safety, while diesel may contain additives for engine performance. For military aviation, JP-8 is the most commonly used fuel. Conventional jet fuels derived from crude oil have a substantial environmental impact, leading to the exploration of more environmentally friendly alternative jet fuels. However, these alternative fuels possess different properties compared to conventional ones. Nanoparticle additives are being tested to enhance the properties of alternative jet fuels [7]

Research on nanoparticles has demonstrated several advantages, including improved stability and an increased surface area-to-volume ratio compared to micron-sized particles. Building on this, a study focused on incorporating aluminium nanoparticles into hydrotreated vegetable oil (HVO), an alternative jet fuel. Nano and micron particles (40 nm and 5 μm) were stably suspended in HVO at a concentration of 0.5 wt%. Pure HVO and Jet A-1 were also included in the study for comparative purposes. Higher furnace temperatures were found to increase the burning rate for all fuels, and the addition of aluminium particles enhanced the combustion of alternative jet fuel. Decreasing particle size and raising furnace temperature further improved the burning rate compared to pure HVO. Pure HVO exhibited a burning rate of nearly $1.75 \text{ mm}^2/\text{s}$ until $t/D_0^2 = 0.35 \text{ s}/\text{mm}^2$ at $T = 1000^\circ\text{C}$. The introduction of nanoparticles at a concentration of 0.5 wt% in HVO resulted in a 24% improvement in the burning rate but led to a shorter lifetime. However, the addition of aluminium particles to HVO also promoted disruptive burning phenomena, with micro-explosions caused by aluminium particles marking the end of the droplet lifetime and

inducing secondary atomization. Micro-explosions increase the fuel surface area which in turn, leads to an increase in the fuel evaporation rate and better air-fuel mixture. [7]

In a separate study, the combustion of kerosene with oxygen-containing nanoparticle additives was investigated. These additives were assembled through electrospray into nitrocellulose-bound composite mesoparticle structures, which exhibited significant improvement in colloidal stability compared to unassembled nanoparticles. However, the combustion of droplets revealed that Al_2O_3 nanoparticles caused minor disturbances in the flame, primarily lengthening flame emission near droplet termination. This emission behaviour resembled that of heated Al_2O_3 , where solid particles remained as liquid burnout completed. In terms of burning rate, the nitrocellulose-bound mesoparticle (100 to 1000 nm particle) architecture did not provide noticeable benefits for Al_2O_3 . Only nanoparticle samples without nitrocellulose increased or had minimal effects on burning rates. Among the metal oxide nanoparticles tested, KIO_4 and CuO mesoparticles demonstrated the most significant burning rate increase but were also the least efficient oxygen carriers by mass. MgO and Al_2O_3 had higher oxygen per mass ratios, but only MgO mesoparticles achieved notable burning rate increases. [8]

In another study, the impact of varying concentrations of Al_2O_3 nanoparticles on the fuel properties of conventional (Jet A-1), alternative (GTL), and a 50-50% blend (G50J50) of jet fuels was examined. The choice of a 50% blend was influenced by the maximum permissible concentration of alternative jet fuel when blended with petroleum jet fuels used by the aviation industry. The study also investigated the non-reacting spray performance under elevated ambient conditions. Al_2O_3 nanoparticles with an average diameter of 13 nm were used at weight concentrations of 2% and 4%. A chemical stabiliser, sorbitan monooleate (commonly known as Span80), was added at a volume concentration of 0.5%. Fuel spray was generated using an aerospace-based pressure swirl nozzle, with varying ambient gas pressures of 100, 500, and 900 kPa, while maintaining an ambient temperature of 400 K for all cases. The findings revealed distinct differences in sheet dynamics between the blended fuel and the pure fuels. At an ambient gas pressure of 100 kPa, the sheet dynamics of the base fuel were more active compared to the nanofuels (2% and 4% weight concentrations). This trend was consistent even at an ambient gas pressure of 900 kPa. The results suggested that, for the pure fuels, nanoparticles at a concentration of 2 wt% had a greater influence on the spray structure compared to a concentration of 4 wt%. The spray cone angle near the nozzle remained similar for all fuels due to its dependence on the internal geometry of the

intake. However, even at low concentrations, nanoparticle dispersion could impact the spray in the near-nozzle region. The earlier disruption of the liquid sheet observed with nanofuels indicated the influence of nanoparticles on the dynamics of the spray liquid sheet. Additionally, ambient pressure had a significant effect on the spray characteristics of the fuels investigated. [9]

Another study explored the use of aviation turbine fuel (ATF)-Al₂O₃ nanofluids to enhance heat transfer performance in potential applications of regeneratively cooled semi-cryogenic rocket engine thrust chambers. Al₂O₃ nanoparticles were employed at concentrations ranging from 0 to 1 wt%. The results demonstrated that for a concentration of 1 wt% Al₂O₃, the thermal conductivity increased by 40%, and viscosity increased by 38%. The specific heats of the nanofluids remained similar across all investigated concentrations. Furthermore, the heat transfer coefficient experienced a 30% increase at 1 wt% Al₂O₃, leading to a subsequent enhancement of 10% in the Nusselt number. The Nusselt number is a measure used in turbine engines to compare the ratio of convective and conductive heat transfer across a boundary. It represents the heat flow parallel to the surface normal and the mean fluid flow. In thermal fluid dynamics, it quantifies the convective and conductive heat transfer at a fluid boundary. A Nusselt number of one (or zero) indicates pure conduction, while values between one and 10 suggest slug flow or laminar flow. Higher Nusselt numbers indicate more active convection, often seen in turbulent flow ranging from 100 to 1000. [10]

1.5. Nanoparticle manufacturing

To produce nanoparticles there are two main methods: top-down and bottom-up. The top-down method usually involves mechanical crushing or milling of the source material. The bottom-up methods, mostly produced by chemical processes, are the most used because they offer better control of the nanoparticles, and therefore this approach is also used in this thesis. [11]

1.5.1. Top-down method for producing nanoparticles

The term 'top-down' describes particle production processes that utilize principles of microsystem technology, focusing on mechanical and physical methods. Traditional approaches to producing nanoparticles through mechanical and physical crushing employ a range of milling techniques. The milling technique is employed in the mechanical production approach to crush microparticles (0.1 to 100 μm particle), specifically for the production of metallic and ceramic nanomaterials. In the case of metallic nanoparticles, conventional source materials like metal oxides are pulverized using high-energy ball mills, which incorporate grinding media made of wolfram carbide or steel. Milling involves thermal stress and consumes significant energy. Prolonged processing can potentially wear down the grinding media, leading to particle contamination. Purely mechanical milling can also be combined with reactive milling, where a chemical or chemo-physical reaction accompanies the milling process. In comparison to chemo-physical production processes, using mills to crush particles results in product powders with a relatively wide range of particle sizes. This method lacks precise control over particle shape. [11]

Laser ablation synthesis in solution (LASiS) is an alternative top-down approach that differs from chemical and other physical methods. LASiS is an eco-friendly technique as it eliminates the need for precursors or reducing chemicals while enabling the production of high-purity colloids without generating harmful waste. In LASiS, a laser beam is directed at a solid target submerged in a liquid, leading to the formation of nanoparticles during the condensation of the resulting plasma plume. By conducting the ablation in a liquid medium, the expansion, cooling, and condensation processes can occur at higher temperature, pressure, and density, resulting in a more confined and controlled plume. Consequently, this method allows to produce smaller and more refined nanoparticles. The size and structure of the synthesized nanoparticles can be precisely manipulated by adjusting the laser parameters and the liquid medium employed. However, it should be noted that currently, this technique has a very high cost. [12]

1.5.2. Bottom-up method for producing nanoparticles

Bottom-up techniques rely on the physicochemical principles of molecular or atomic self-organization. This methodology enables the creation of specific and intricate structures from atoms or molecules, offering enhanced control over size, shape, and size ranges. It encompasses various processes such as aerosol methods, precipitation reactions, and sol-gel processes. [11]

Aerosol processes are widely used in industrial-scale applications to produce nanomaterials in powder or film form. These processes involve converting the product material into a vapor state through chemical or physical means, resulting in the formation of nanoparticles. Initial nanoparticles are created through homogeneous nucleation and can exist in liquid or solid states. Particle growth occurs through mechanisms such as condensation, surface chemical reactions, coagulation, and coalescence. Examples of gas phase processes include those implemented in flame, plasma, laser, and hot wall reactors, which produce materials like fullerenes and carbon nanotubes. [11]

Droplets can also be utilised to generate particles using various techniques like centrifugal forces, compressed air, sonic waves, ultrasound, vibrations, and electrostatics. These droplets are then converted into powder either through direct pyrolysis, involving thermal cleavage of compounds, or direct reactions with gases. In spray pyrolysis, for instance, droplets of the source material are exposed to high temperatures, leading to vaporization or decomposition reactions, and the resulting particles are collected on filters. [11]

In a wet-chemical synthesis of nanomaterials, lower temperatures are typically used compared to gas phase synthesis. Among the key processes in liquid-phase nanomaterial production, precipitation, sol-gel processes, and hydrothermal syntheses are particularly important. [11]

Precipitation processes involve precipitating solids from solutions containing metal ions. This versatile method can produce metal oxides, non-oxides, and metallic nanoparticles by inducing particle precipitation through a precipitating agent. After filtration, the precipitate undergoes thermal post-treatment. Particle size, distribution, crystallinity, and morphology are determined by reaction kinetics influenced by factors such as concentration, temperature, pH, material addition sequence, and mixing. Self-assembled membranes like microemulsions, bubbles, micelles, and liposomes act as nanoreactors, allowing precise size

control and preventing agglomeration. Microemulsion processes are commonly used for pharmaceutical and cosmetic nanoparticles. [11]

Sol-gel syntheses are wet-chemical processes that produce porous nanomaterials, ceramic nanostructured polymers, and oxide nanoparticles under mild conditions and relatively low temperatures. The process involves transforming a liquid sol state containing solid particles into a solid gel state through a sol-gel transformation. This transformation cross-links nanoparticles, forming a gel with bulk properties. In sol-gel processes, organic substances are added to initiate the transformation of, for example, an alkoxide solution into an organometallic compound. Catalysts adjust the pH value and trigger the alkoxide transformation, followed by hydrolysis, condensation, and polymerization reactions leading to gel formation. The porous gel structure provides a large surface area per gram. The reactions are influenced by factors such as initial solution composition, catalyst type and amount, temperature, reactor, and mixing geometry. Sol-gel processes can coat surfaces of any shape, and thicker layers can be created through repeated wetting and drying steps. The sol-gel process offers a high degree of control over nanoparticle size and morphology through the manipulation of reaction parameters, including precursor concentration, hydrolysis rate, and condensation rate. This precise control enables the production of nanoparticles with customized properties by incorporating dopants or additives during the sol-gel process. These tailored properties can include enhancements in optical characteristics, magnetic behaviour, or catalytic activity, among others. [11]

1.5.3. Green synthesis

Typically, the chemical techniques employed are costly and involve the use of dangerous and harmful chemicals, posing risks to the environment. For example, precursor compounds can be aluminium isopropoxide or zinc acetate, whereas sodium borohydride and hydrazine are used as reducing agents. In contrast, the biosynthetic approach offers a safe, biocompatible, and environmentally friendly method to produce nanoparticles utilizing plants and microorganisms. This synthesis can be performed using fungi, algae, bacteria, and plants, among others. Various components of plants, including leaves, fruits, roots, stems, and seeds, have been utilised in the synthesis of nanoparticles due to the presence of

phytochemicals in their extracts, which serve as stabilizing and reducing agents, where nitrate precursors are preferred as metal source. [13]

Green synthesis incorporating plant extracts in chemical processes is cost-effective and manageable. In most common nanoparticle synthesis, the plant sample undergoes a simple procedure involving washing with distilled water followed by boiling to get the plant extract. Then the plant extract is cleaned and mixed with precursors while it changes colour. This can be carried out at room temperature or elevated temperatures. The resulting product is rinsed with a solvent. Through centrifugation, the nanoparticles are separated from the solvent solution. Green synthesis of nanoparticles using plants is environmentally friendly as it does not generate toxic chemical by-products. [13]

1.6. Safety, risks, and drawbacks of using nanoparticles as fuel additives

The potential toxicity and health effects of nano-additives, like many other nanomaterials, present a significant obstacle to their widespread commercial use. Several *in vivo* and *in vitro* studies have established a strong connection between nanoparticles and toxicity. Despite the advantages they offer, nanoparticles have exposed humans, animals, and plants to potential toxicity through various applications of nanotechnology. [14]

Nanoparticles can enter the human body through inhalation, ingestion, skin absorption, injection, and implantation. Their small size, ease of penetration, biocompatibility, and potential to breach the placental barrier has raised concerns about their negative impact on human health, particularly on reproductive systems and foetal well-being. Preliminary research on anthropogenic nanoparticles, such as those found in diesel exhaust, reveals that regular exposure leads to their aggregation and attachment to human cells, disrupting normal physiological processes. Additionally, nanoparticles have been associated with pulmonary injury, hepatotoxicity, immuno-nanotoxicity, neurotoxicity, renal toxicity, and permanent damage to the testes in animals. [14]

Nanomaterials have the ability to agglomerate, forming larger particles or longer fiber chains, which alters their characteristics and can potentially affect their behaviour in both indoor and outdoor environments. This alteration may impact their exposure and entry into the human body. Due to their large surface area, high surface activity, unique shape, tiny diameters, or ability to decompose into smaller particles after deposition, nanoparticles can

deposit in the respiratory system and exhibit toxicity related to their nanostructure and composition. [14]

Nanoparticles have a high deposition efficiency in the lungs of healthy individuals, and even higher deposition efficiencies in those with asthma or chronic obstructive pulmonary disease. Overexposure to nanoparticles has been proven to cause DNA and reproductive damage, cytotoxicity, and even cancer. It is important to note that efforts have been made to mitigate the toxicity of nanoparticles. Some approaches include the use of degradable nanoparticles, next-generation lipids, surface coating, doping, and modification of surface properties. Doping nanoparticles with substances such as aluminium, titanium, and iron has been found to reduce nanoparticle dissolution and the release of toxic ions, resulting in altered reactive surfaces and decreased generation of reactive oxygen species. [14]

The addition of more nanoparticles to the fuel increases the potential risks associated with them. Insufficient combustion or mishandling of nanofuel can result in the excessive release of nanoparticles into the environment. To mitigate the release of nanoparticles caused by incomplete combustion, various methods have been developed. These methods include the use of diesel particulate filters (DPF), selective catalytic reductions (SCR), exhaust treatment using photocatalytic technology, exhaust gas recirculation (EGR), and combinations of these approaches. [14], [15], [16]

Exhaust gas recirculation is a widely used automotive method primarily employed to reduce NO_x emissions resulting from high combustion temperatures. It functions by recirculating a small portion of the exhaust gas back into the combustion chamber via the intake manifold, thereby diluting the air-fuel mixture and lowering temperatures. EGR operates in three conditions: high flow for mid to high-speed ranges, low flow for low speeds and lighter loads, and no flow during engine warm-up and idle throttle. However, excessive EGR can negatively impact engine performance and cause knocking. The EGR ratio determines the volume of recirculated exhaust gas. Notably, factors influencing NO_x emissions include the reduced heat capacity of air, lower oxygen concentration inside the cylinder, and decreased combustion speed. While EGR primarily focuses on NO_x reduction, it indirectly impacts nanoparticle filtration by altering combustion conditions and lowering overall emissions. Increasing the rate of EGR leads to a reduction in NO_x levels. However, insufficient oxygen supply causes a decrease in the air-fuel ratio, resulting in reduced brake thermal efficiency at higher loads. As the EGR flow rate increases, the intake of fresh air from the atmosphere

decreases, leading to a leaner mixture due to the lack of fresh air and increased fuel. Consequently, engine performance declines. [16]

Combining EGR with diesel particulate filters allows the trapping of soot particles, enabling only clean gases to pass through the EGR into the combustion chamber. HC and CO levels enter the combustion chamber, where they are completely burned. However, due to the high combustion chamber temperature, NO_x levels also increase. Therefore, the combination of particulate matter trapping in the DPF and allowing other gases into the combustion chamber has a positive effect with an EGR rate of 10%. At higher EGR rates, back pressure occurs in the DPF system due to soot build-up, which hinders soot elimination under lower load conditions when gas temperatures are low. [16]

Combining SCR with EGR reduces NO_x levels by converting them into nitrogen gas. However, combining SCR with EGR also increases the amount of CO₂ entering the combustion chamber, leading to incomplete combustion and higher levels of HC and CO in the exhaust gases. An EGR rate of 10% with SCR demonstrates a positive impact without compromising engine performance. [16]

The optimal combination depends on the specific gas emissions to be reduced. To primarily reduce NO_x, a combination of 10-20% EGR with the SCR system is preferred. On the other hand, to reduce HC, CO, and soot, a combination of 10-20% EGR with a DPF system is recommended, which yields moderate improvements in emission reduction. Implementing EGR in combination with DPF and SCR systems can effectively reduce soot and NO_x at low EGR rates. [16]

2. MATERIALS AND METHODOLOGY

This chapter provides a detailed description of the materials and methods employed in this research. The procedures are outlined systematically to enable reproducibility and to ensure clarity regarding the research approach. The methods chosen for this study were selected based on their proven efficacy in similar research contexts and their alignment with the research objectives. The study was designed as quantitative experimental research conducted over twelve months. It was carried out in a controlled laboratory setting to ensure precision and accuracy in data collection. The materials utilised in this study included high-precision lab equipment, specific reagents required for chemical analysis, and software for data processing and statistical analysis. The research focused on investigating the effects of nanoparticle additives in jet fuel, aiming to enhance fuel efficiency, and performance, and reduce harmful emissions. The following sections detail the specific methodologies employed in this study. Section 2.1 details the laboratory equipment utilised, encompassing the engine test stand and associated software. Section 2.2 describes the methods for nanoparticle preparation, including analyses of nanoparticles to ensure their quality and characteristics. Section 2.3 outlines the experimental procedures and protocols for engine testing.

2.1. Used laboratory equipment and software

Digital magnetic stirrer with heating plate (LBX H03D)

The H03D laboratory stirrer (figure 2.1.a) is constructed with a housing made of ABS incorporating fire retardant materials, offering resistance against weak acids and alkalis. The hotplate is ceramic-coated, and it features an LED display for monitoring both temperature and stirring speed. The stirring speed is adjustable within the range of 200 to 1500 rpm, while the temperature on the plate can be adjusted up to 280°C. The heat plate has a heating power of 515 W. The stirrer operates with a maintenance-free DC brushless motor, suitable for beakers with a diameter of less than 135 mm and magnetic bars up to 50 mm in length. External dimensions are 260 x 150 x 80 mm. [17]

Multi-function centrifuge (Ohaus Frontier FC5707)

The FC5707 centrifuge (figure 2.1.b) has a touch-wheel control interface. The centrifuge comes with a pre-installed 8 x 15 ml angle rotor capable of processing both round and conical bottom tubes, including common blood tubes. Additionally, it can be adapted for use with 7-, 5-, and 1.5/2.0-ml tubes when used with compatible accessories. The dimensions of the centrifuge are 277 × 356 × 236 mm, with a weight of 10 kg. It offers a speed range of 200 to 6800 rpm and a maximum relative centrifugal force (RCF) of 4445 x g. [18]

Analytical balance (Kern ALJ 200)

The ALJ 200 analytical balance (figure 2.1.c) is equipped with an integrated ALJ-A03 Ionizer, facilitating the neutralization of electrostatic charges without necessitating a separate device. Featuring a short stabilization time of 10 seconds (6 seconds under laboratory conditions), the balance ensures expedited and efficient operation. Its interface is characterized by a clear graphics display available in multiple languages. Additionally, the inclusion of a large glass draught shield facilitates easy access to weighed items. With a maximum weighing capacity of 82/220 grams and a readability of 0.00001 grams, it accommodates a diverse array of measurement units. Operating within an ambient temperature range of 5°C to 35°C, it features a stainless-steel weighing plate, a glass draught shield, and a plastic housing, ensuring durability and reliability. The balance's dimensions are 210 x 340 x 330 mm, with an approximate net weight of 7 kg. [19]

Ultrasonic cleaner (LBX ULTR-0L8-001)

The ULTR-0L8-001 ultrasonic cleaner is equipped with a resilient 0.8 L stainless steel bath, supplemented by a digital interface facilitating precise timing observations. Operating at a frequency of 40 kHz, the timer affords customizable cleaning cycles spanning from 0 to 30 minutes. The bath dimensions are 150 x 85 x 65 mm, while the basket dimensions are 135 x 70 x 40 mm. With a rated ultrasound power output of 50 W. [20]

UV/Visible spectrophotometer (VWR UV-1600PC)

The UV-1600PC UV/Visible spectrophotometer (figure 2.1.d) offers various measuring modes including photometry, quantitation, and kinetics. The instrument features a dot matrix LCD for clear visualization of data. Employing a single-beam optical design, it ensures accuracy with a photometric accuracy of ±0.5%T or 0.005A @ 1A. The photometric range

spans from 0 to 200% T, -0.3 to 3.0 A, and 0 to 9999 C. Photometric stability is maintained at ± 0.002 A/h (at 500 nm), while wavelength accuracy stands at ± 0.5 nm with a wavelength range of 190 to 1100 nm. Users can operate the spectrophotometer in English, German, Spanish, or French, enhancing accessibility. It has a memory capacity for storing 200 results and 200 standard curves. Spectral bandwidth is set at 4 nm, with stray light kept minimal at $\pm 0.05\%$ T (220; 360 nm). The instrument's dimensions are 490×360×240 mm and weight 14 kg. [21]

Laboratory oven (Mettler MMT-UN30)

The laboratory oven MMT-UN30 (figure 2.1.e) has sophisticated ventilation and control systems, coupled with over-temperature protection and calibrated heating mechanisms. Offering a temperature range spanning from a minimum of 5°C above ambient temperature to +300°C. The oven has increments of 0.1°C up to 99.9°C and 0.5°C thereafter. The interior, reinforced with deep-drawn ribbing and integrated large-area heating elements on all sides, has a volumetric capacity of 32 litres. The interior dimensions are 400 x 320 x 250 mm; therefore, the oven accommodates up to three internals, each capable of bearing a maximum load of 20 kg. [22]

Spectrometer (ThermoFisher Nicolet iS10)

The Nicolet iS10 Fourier-transform infrared spectroscopy (FTIR) Spectrometer (figure 2.1.f) is designed to meet ISO/GLP requirements and undergoes performance verification according to ASTM E1421 standards. It features a standard KBr/Ge mid-infrared optimized beam splitter, with an optional XT-KBr/Ge extended range mid-infrared splitter available. Components include user-replaceable mid-infrared Ever-Glo and Tungsten/halogen sources accessible from the sample compartment. The spectrometer interfaces with a PC via USB 2.0, and its laser source is HeNe. Spectral ranges vary depending on the beam splitter type, with optimized ranges from 7800 to 350 cm^{-1} and extended ranges from 11,000 to 375 cm^{-1} . Spectral resolution is better than 0.4 cm^{-1} . It is compatible with SMART Accessories, TGA-IR, Continuum Microscope, Photoacoustic, and most standard accessories, catering to various analytical applications such as biodiesel blending analysis, gemstone analysis, polymer analysis, QA/QC, pharmaceutical analysis, and forensics. The instrument dimensions are 570×550×250 mm and weight 33 kg. [23]



Figure 2.1. Used laboratory equipment LBX H03D (a), Ohaus Frontier FC5707 (b), Kern ALJ 200 (c), VWR UV-1600PC (d), Memmert MMT-UN30 (e), ThermoFisher Nicolet iS10 (f).

Scanning electron microscope (FEI QUANTA 250)

The scanning electron microscopy (SEM) study was performed in collaboration with the LMGP laboratory (University Grenoble Alpes – Minatec, France) because LEO / ZEISS 1430VP was not working properly during the time of this study. The SEM study was carried out on a FEI QUANTA 250 environmental SEM FEG operating at energy ranging from 3 to

15 kV. SEM is specialized for high-resolution imaging and analysis of small three-dimensional samples, offering exceptional capabilities for both imaging and analytical measurements. Its field emission electron gun provides high energy resolution and minimal beam astigmatism, suitable for imaging and experiments. Operating in low or high-voltage modes, it facilitates analyses such as EDX and WDS. Detectors such as EDX offer high sensitivity for elemental analysis. Automated software packages optimize data collection, processing, and analysis. [24]

Engine test stand (TA-8)

The engine tests utilised the Tu-134 airplane auxiliary power unit (APU) turbine engine TA-8. TA-8 (figure 2.2) has a power output of 128 kW and a specific fuel consumption of 1.09 kg per kWh. With a weight-to-power ratio of 1.44 kg per kW (excluding the alternator), it operates effectively up to 5,000 meters and has a service life of 2,000 hours or 8,000 starts. The APU's bleed air parameters include a flow of 0.8 kg per second, generating 10 kVA of electrical power with a pressure of 3.4 kg per cm² when supplying bleed air. Without the air bleed, the electrical power output increases to 25 kVA, with the bleed air temperature regulated at 210°C for optimal performance and safety.

For data monitoring, the DEWE-43A data acquisition system was employed. The DEWE-43A offers versatility with its 8-channel USB data acquisition system, featuring a good price/performance ratio and a compact hand-size footprint. It includes 8 universal analogue inputs, 8 digital/counter/encoder inputs, and two high-speed CAN bus inputs. [25]

To test exhaust emissions, the Bosch BEA 350 combination petrol and diesel emissions analyser was used. [26]

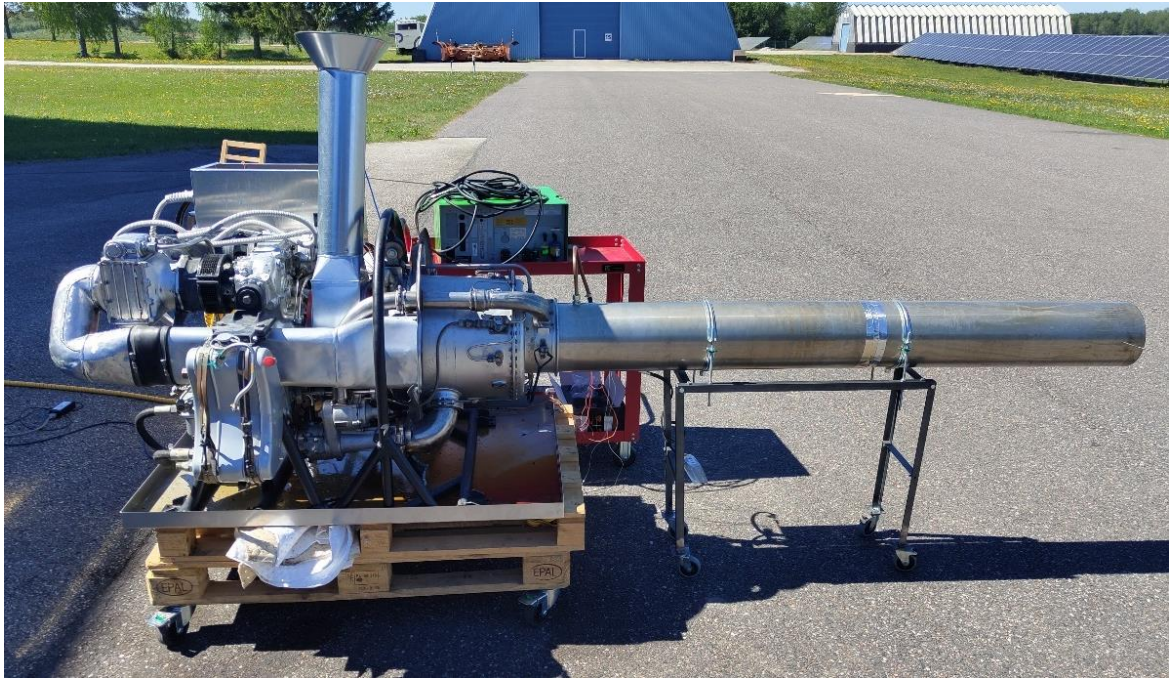


Figure 2.2. Auxiliary power unit test stand (TA-8) in the Estonian Aviation Academy Department of Aeronautical Engineering.

Used software

Absorption and Tauc plots were generated using OriginPro 2024 software. OriginPro features a user-friendly interface suitable for beginners and allows for advanced customization as users gain familiarity. Graphs and analysis results in OriginPro can automatically update with data or parameter changes, facilitating the creation of templates for repetitive tasks and enabling batch operations directly from the interface without programming. Users have the option to enhance the capabilities of their software by installing additional applications from the website and integrating with various other software platforms. Alternatively, they can develop custom routines utilising scripting and C languages, embedded Python, or the R console. [27]

For engine tests, DewesoftX data acquisition and signal processing software were employed. DewesoftX is a renowned software known for data acquisition and signal processing, widely utilised across various test and measurement applications in all industries. It serves as a standard for signal measurement, data recording, signal processing, and data visualisation, contributing to efficient and comprehensive data analysis in diverse testing scenarios. [28]

2.2. Preparation of nanoparticles

2.2.2. Synthesis of Al₂O₃ and ZnO nanoparticles

To produce Al₂O₃ and ZnO nanoparticles, five different syntheses were performed. Syntheses were performed under different conditions (table 2.1), that were changed to improve the yield.

Table 2.1. Syntheses conditions

Synthesis		1	2	3	4	5
Precursor	Al ₂ O ₃	0.01 mol (Al(NO ₃) ₃ , 9H ₂ O)	0.01 mol (Al(NO ₃) ₃ , 9H ₂ O)	0.01 mol (Al(NO ₃) ₃ , 9H ₂ O)	n/a	0.01 mol (Al(NO ₃) ₃ , 9H ₂ O)
	ZnO	0.01 mol (Zn(NO ₃) ₂ , 8H ₂ O)	0.01 mol (Zn(NO ₃) ₂ , 8H ₂ O)	0.01 mol (Zn(NO ₃) ₂ , 8H ₂ O)	n/a	0.01 mol (Zn(NO ₃) ₂ , 8H ₂ O)
Activator	Al ₂ O ₃	n/a	n/a	n/a	0.005 mol	0.005 mol
	ZnO	n/a	n/a	n/a	0.005 mol	0.005 mol
Plant extract	Al ₂ O ₃	50 ml	n/a	50 ml	n/a	50 ml
	ZnO	50 ml	n/a	50 ml	n/a	50 ml
Supernatant	Al ₂ O ₃	n/a	120 ml	n/a	100 ml	n/a
	ZnO	n/a	110 ml	n/a	150 ml	n/a
Water	Al ₂ O ₃	100 ml	80 ml	100 ml	n/a	100 ml
	ZnO	100 ml	90 ml	100 ml	n/a	100 ml
Method	Al ₂ O ₃	LBX H03D	Memmert MMT-UN30	LBX H03D	LBX H03D	Memmert MMT-UN30
	ZnO	LBX H03D	LBX H03D	Memmert MMT-UN30	LBX H03D	Memmert MMT-UN30
Temperature	Al ₂ O ₃	130°C	90°C	250°C 15 min, 220°C 60 min	220°C	90°C
	ZnO	130°C	250°C	90°C	220°C	90°C
Stirring during synthesis	Al ₂ O ₃	600 rpm	n/a	600 rpm	600 rpm	n/a
	ZnO	600 rpm	600 rpm	n/a	600 rpm	n/a
Synthesis time	Al ₂ O ₃	75 min	75 min	75 min	75 min	75 min
	ZnO	75 min	75 min	75 min	75 min	75 min
Drying time	Al ₂ O ₃	48 h	n/a	120 h	n/a	120 h
	ZnO	48 h	n/a	120 h	48 h	120 h

First synthesis

Preparation for the first synthesis started with the preparation of 10 g of crushed sunflower seeds in 200 ml of distilled water inside a 250 ml beaker. The solution was put onto H03D. The heating plate was set to 140°C and stirred at 1200 rpm by a magnetic stirrer for one

hour. After the solution containing sunflower seed extract cooled down, the solution was filtered to remove solid particles. Following this step, the solution was centrifuged for 4 min at 6800 rpm with FC5707 to remove the smallest particles present in the solution.

For the synthesis, a solution containing 0.01 mol of aluminium nitrate nonahydrate 99+% ($\text{Al}(\text{NO}_3)_3 \cdot 9\text{H}_2\text{O}$) with a molecular weight of 375.13 g/mol and 0.01 mol of zinc nitrate hexahydrate 98% ($\text{Zn}(\text{NO}_3)_2 \cdot 6\text{H}_2\text{O}$) with a molecular weight of 297.46 g/mol were prepared. To prepare the solutions, 3.751 g of aluminium nitrate and 2.975 g of zinc nitrate were dissolved in 100 ml of distilled water respectively (measured with ALJ 200). Both nitrate solutions were stirred with H03D for 4 min at 1000 rpm. 50 ml of sunflower seed extract solution was then slowly added to both zinc and aluminium nitrate solutions while being stirred at 600 rpm. The resulting solutions were heated and stirred for 75 minutes. The heating plate was set to 130°C and stirred at 600 rpm. After that, the solutions were left to cool for one hour.

After cooling, both solutions were put into 15 ml centrifuge test tubes and centrifuged with FC5707 for 6 min at 6800 rpm for zinc solution, and 2 x 6 min at 6800 rpm for aluminium solution. The liquid was separated from the solid particles. The pH of the remaining supernatants was measured with a pH meter PH-983. The nanoparticles were left in a drying oven for 2 days at 45°C. After drying, Al_2O_3 and ZnO nanoparticles were crushed into a fine powder by using a laboratory mortar and pestle.

Second synthesis

For the second synthesis, the remaining supernatant (solution that remain following the first centrifugation after the synthesis completion) from the first synthesis was used. Both Al_2O_3 and ZnO supernatants were filtered and put into 250 ml beakers. For the synthesis, similarly to the first synthesis, solutions of 0.01 mol aluminium nitrate nonahydrate and 0.01 mol of zinc nitrate hexahydrate were prepared. For Al_2O_3 synthesis 120 ml of supernatant and 80 ml distilled water with 3.751 g of aluminium nitrate was prepared. For ZnO synthesis, 110 ml of supernatant and 90 ml of distilled water with 2.975 g of zinc nitrate were prepared. Bringing the total up to 200 ml for both solutions. Both solutions were then stirred with a magnetic stirrer for 5 min at 600 rpm.

Two different methods of heating were applied after stirring. The beaker containing the solution of aluminium nitrate was put into a steel pressure vessel that was put into MMT-UN30. The oven was set to 90°C for 75 minutes. The beaker containing zinc nitrate solution

was covered with aluminium foil and heated with H03D, heating plate was set to 250°C and stirred at 600 rpm for 75 minutes. After synthesis, the solutions were left to cool down overnight. After cooling a UV light was used to check the presence of nanoparticles inside the solution. Solutions were put into 15 ml centrifuge test tubes and centrifuged for 15 min at 6800 rpm. After that, both solutions were put into 2 ml centrifuge test tubes and centrifuged for 15 min at 6800 rpm.

The following week, plant extract containing ZnO nanoparticles was put into 15 ml centrifuge test tubes and centrifuged for 3 hours at 6800 rpm. After the centrifuge, test tubes were placed into a beaker to see if the nanoparticles would fall into the bottom of the test tubes.

Third synthesis

The third synthesis of nanoparticles started with preparing 15 g of crushed sunflower seeds in 250 ml of distilled water inside a 250 ml beaker. The solution was put into an autoclave that was put into MMT-UN30. The oven was set to 90°C for 90 minutes. After that, the plant extract solution was left to cool down overnight. The solution was filtered to remove solid particles. Following this step, the solution was centrifuged for 4 min at 6800 rpm with FC5707 to remove all small remaining nanoparticles present in the solution.

For the synthesis, similarly to previous syntheses, solutions of 0.01 mol aluminium nitrate nonahydrate and 0.01 mol of zinc nitrate hexahydrate were prepared. Both nitrate solutions were stirred with H03D for 4 min at 1000 rpm. 50 ml of sunflower seed extract solution was then slowly added to both zinc and aluminium nitrate solutions while being stirred at 600 rpm.

After stirring the beaker containing the aluminium nitrate solution was covered with a glass test plate and wrapped with aluminium foil. Then it was heated under magnetic stirring at 600 rpm with the heating plate set to 250°C for 75 minutes. After 15 minutes the solution started to bubble and boil over the glass beaker, then the heating plate was lowered to 220°C, until the end of synthesis to stop the solution from boiling over.

The solution containing zinc was put into a steel pressure vessel that was put into a laboratory oven MMT-UN30. The oven was set to 90°C and 75 minutes. After synthesis, the solutions were left to cool down overnight.

After cooling both solutions were put into 15 ml centrifuge test tubes and centrifuged for 10 minutes at 4500 rpm. The liquid was separated from the solid nanoparticles. The

nanoparticles were left in a drying oven for 5 days at 45°C. After drying Al₂O₃ and ZnO nanoparticles were crushed into a fine powder by using laboratory mortar and pestle.

Fourth synthesis

For the fourth synthesis, Al₂O₃ and ZnO supernatants from the third synthesis were used. Both supernatants were put into 250 ml beakers that were covered with a glass test plate and wrapped with aluminium foil. The beakers were put onto H03D set to 220°C and stirred at 600 rpm. Then 0.005 mol of activator was added drop by drop to both solutions. Both solutions were put on the heating plate for 75 minutes with the heat plate set to 220°C and stirred at 600 rpm. After synthesis, the solutions were left to cool overnight.

After cooling ZnO solution was put into 15 ml centrifuge test tubes and centrifuged for 15 minutes at 4500 rpm. The liquid was separated from the solid particles. The nanoparticles were left in a drying oven for 2 days at 45°C. After drying ZnO nanoparticles were crushed into a fine powder by using a laboratory mortar and pestle.

Fifth synthesis

The fifth synthesis started with the preparation of the activator solutions (possible patent application). For that two solutions of 0.005 mol of activator and 50 ml of distilled water were mixed. Then, similarly to previous syntheses, solutions of 0.01 mol aluminium nitrate nonahydrate and 0.01 mol of zinc nitrate hexahydrate were prepared. 50 ml of sunflower seed extract solution was then slowly added to both aluminium and zinc nitrate solutions while being stirred at 600 rpm. Then 50 ml of activator solution was added drop by drop to both solutions.

For the fifth synthesis, both aluminium and zinc solutions were put into a steel pressure vessel that was put into MMT-UN30. The oven was set to 90°C and 75 minutes. After synthesis, the solutions were left to cool down overnight.

After cooling both solutions were put into 15 ml centrifuge test tubes and centrifuged for 15 minutes at 4500 rpm. Al₂O₃ solutions were also centrifuged for 15 minutes at 4500 rpm. For the ZnO solution, the liquid was separated from the solid particles. The nanoparticles were left in a drying oven for 5 days at 45°C. After drying ZnO nanoparticles were crushed into a fine powder by using a laboratory mortar and pestle.

2.2.3. UV-vis spectrophotometer analyses

The absorbance measured in UV-visible spectroscopy provides insights into a substance's molecular structure, concentration, and interactions, while analysis of Tauc plots derived from absorbance data allows for the assessment of its bandgap energy. While the bandgap energy provides insights into optical properties and applications, it's just one component in a comprehensive characterisation process, requiring additional analytical techniques for definitive substance identification.

To measure the absorbance of the nanoparticles, the samples were prepared for UV-vis spectrophotometer analyses. For that, both Al₂O₃ and ZnO nanoparticle solutions containing 5 mg of nanoparticles in 5 ml of isopropanol were prepared. To promote a better dispersion of the nanoparticles in the isopropanol, the samples were put into ULTR-0L8-001 for 100 s. After the ultrasonic bath, the samples were put into UV-1600PC to measure the absorbance. Samples were scanned from 1000 – 200 and 500 – 200 nm with an interval of 2 nm. Before the scans, both samples were shaken so that the nanoparticles were suspended at the beginning of the scan.

The absorbance of the nanoparticles with Jet A-1 fuel was also measured. For that, both Al₂O₃ and ZnO nanoparticle solutions containing 10 mg of nanoparticles in 250 ml (40 ppm) of Jet A-1 were prepared. A sample of ZnO nanoparticle solution containing 25 mg of nanoparticles in 250 ml (100 ppm) of Jet A-1 was also prepared. To promote a better dispersion of the nanoparticles in the Jet A-1, the nanoparticles were further crushed into even finer powder by using laboratory mortar and pestle. During the crushing few drops of Jet A-1 were added to aid in the crushing of the nanoparticles. To promote the nanoparticle dispersion in Jet A-1, the samples were put onto the heating plate with the temperature set to 80°C, stirring at 950 rpm. After stirring for 20 minutes the heating was turned off and the samples were left to stir overnight at 950 rpm. Using the spectrophotometer, samples were scanned from 1000 – 200 with an interval of 2 nm. Tauc Plots were calculated from the absorbance [29].

To measure the absorbance of the nanoparticles from the third synthesis, the samples were prepared for UV-vis spectrophotometer analyses. For that, both ZnO and Al₂O₃ nanoparticle solutions containing 5 mg of nanoparticles in 5 ml of isopropanol were prepared. The samples were put into UV-1600PC to measure the absorbance. Samples were scanned from 1000 – 200 with an interval of 2 nm. Before the scans, both samples were shaken so that the

nanoparticles were suspended at the beginning of the scan. Tauc Plots were calculated from the absorbance.

2.2.4. Heating plate temperature calibration

To get an accurate correlation between the set temperature of the heating plate and the actual temperature inside the beaker, an experiment was conducted. H03D and a 250 ml glass beaker were used. The beaker was filled with 150 ml of distilled water, partly covered with paraffin film. A magnetic stirrer, set at 600 rpm was used for stirring and a mercury thermometer was used for measuring the temperature inside the beaker. The heating plate temperature was set to 130°C and then increased by 10°C intervals, up to 280°C, when the temperature inside the beaker stabilized.

For the second experiment, a pressure cooker pot was used. The same 250 ml glass beaker was filled with 150 ml of distilled water, covered with paraffin film, and placed inside the pressure cooker. The temperature inside the beaker was measured with the heating plate set at 140°C and 200°C.

2.2.5. Preparation of fuel samples for analyses and engine tests

Before being mixed with the fuel, the nanoparticles were placed inside a mortar. To facilitate the crushing process, a few drops of Jet A-1 were added to the nanoparticles, after which they were crushed using a pestle. This method was consistently employed for the preparation of nanoparticle additive fuel in all subsequent experiments.

For fuel composition testing, four fuel samples were prepared. The first sample was pure Jet A-1 without nanoparticles. The second sample was 250 ml of Jet A-1 containing 10 mg (40 ppm) of Al₂O₃ nanoparticles from the first synthesis. The third sample was 250 ml of Jet A-1 containing 25 mg (100 ppm) of ZnO nanoparticles from the first synthesis. The fourth sample was 200 ml of Jet A-1 containing 8 mg (40 ppm) of ZnO nanoparticles from the fifth synthesis.

For fuel characterization, the first sample of Jet A-1 without nanoparticles and the third sample of Jet A-1 containing 100 ppm of ZnO nanoparticles were submitted to the Estonian

Environmental Research Centre (Eesti Keskkonnauuringute Keskus) for analyses. The distillation characteristics were determined following the EVS-EN ISO 3405 standard. The flash point was measured according to the EVS-EN ISO 2719 standard, the density was evaluated following the EN ISO 12185 standard, and the cetane index was calculated using the EVS-EN ISO 4264 standard.

For the engine test, two new fuel samples were prepared. One sample was 4 Liters of pure Jet A-1 without nanoparticles. The other sample was 4 Liters of Jet A-1 containing 400 mg (100 ppm) of ZnO nanoparticles from the fourth synthesis.

2.2.6. FTIR analyses

Five samples were prepared for FTIR analyses. FTIR analyses provide information about the molecular composition of the top layer of a substance, offering insights into its surface chemistry and interactions. Samples from the third, fourth, and fifth synthesis were utilised for ZnO, while samples from the first and third synthesis were employed for Al₂O₃. The absorption of these samples was measured using the ThermoFisher Nicolet iS10 spectrometer.

2.2.7. SEM analyses

The SEM analyses utilized ZnO nanoparticle samples identical to those employed in the FTIR investigations. Specifically, the ZnO samples originated from syntheses three, four, and five. High-resolution images of the samples were captured using the FEI QUANTA 250 environmental SEM FEG, facilitating a detailed examination of their morphology characteristics and composition. This consistent approach ensured the comparability and reliability of the SEM data across the different nanoparticle synthesis batches.

2.2.8. XRD analyses

The X-ray diffraction (XRD) analyses were conducted using a Bruker D8 Discover diffractometer (Bruker AXS, Germany) with $\text{CuK}_{\alpha 1}$ radiation ($\lambda = 0.15406 \text{ nm}$) selected by a Ge (111) monochromator and LynxEye detector on ZnO nanoparticle samples identical to those studied by FTIR and SEM. Specifically, the ZnO samples originated from syntheses three, four, and five, ensuring consistency across all three analytical techniques. These samples were prepared and sent off for XRD analysis to identify their crystalline structure.

2.3. Engine tests

The jet engine tests were conducted at the Estonian Aviation Academy Department of Aeronautical Engineering, situated within the Tartu Airport premises. The tests were carried out utilising the TA-8 APU. Each engine test lasted for 90 seconds, with a 15-minute interval between tests to allow for engine and sensor cooling, ensuring consistent results. Two tests were conducted using pure Jet A-1 fuel, while another two utilized Jet A-1 fuel enriched with 100 ppm of ZnO nanoparticles from the fourth synthesis. Throughout the tests, the engine operated at 100% speed without any load applied. Sensor readings were collected 60 seconds after the engine reached its operational mode following startup. Data from inlet airspeed, inlet temperature, inlet air pressure, exhaust airspeed, exhaust temperature, and exhaust pressure sensors were recorded using the DEWE-43A data acquisition system paired with DewesoftX software. Air mass in and air mass out were calculated from airspeed and air pressure. Additionally, emissions analysis was performed using the Bosch BEA 350 emissions analyser to monitor HC, NO_x , CO_2 , and O levels in the exhaust gases.

3. RESULTS AND DISCUSSION

This chapter presents and discusses the findings of the research on the effects of nanoparticle additives in jet fuel. The results are organised to provide a clear understanding of the outcomes and their implications. The chapter begins with the synthesis of nanoparticles, ensuring their quality and characteristics, followed by various analyses of the nanoparticles. Subsequently, the results of fuel analyses are presented, along with the outcomes of engine tests.

The discussion section places these findings in the context of the research hypotheses and objectives, examining how nanoparticle additives affect jet fuel performance and efficiency while comparing them to previous studies. Moreover, it explores the potential implications for the aviation industry, considering both the advantages and challenges associated with the adoption of nanoparticle-enhanced jet fuels.

Section 3.1 comprehensively presents the results of nanoparticle synthesis, analyses, and the modifications of fuel properties due to nanoparticle additives. Section 3.2 discusses the outcomes of engine testing, covering performance improvements and emission reductions.

3.1. Results of the preparation of the Nanoparticles

3.1.1. Results of the Al₂O₃ and ZnO nanoparticles syntheses

Differences in synthesis conditions resulted in significantly different results, underscoring the sensitivity of the nanoparticle formation process to factors like temperature, reaction duration, and the inclusion of an activator (table 3.1). In this thesis, Al₂O₃ nanoparticles from the first and third syntheses will be denoted as Al₂O₃ PE1 and Al₂O₃ PE3, respectively. Similarly, ZnO nanoparticles from the third, fourth, and fifth syntheses will be referred to as ZnO PE3, ZnO PE4 SN, and ZnO PE5 Act, respectively.

Table 3.1. Syntheses results

Synthesis		1	2	3	4	5
Colour of the supernatant	Al ₂ O ₃	yellow translucent	yellow translucent	yellowish	yellowish	yellowish
	ZnO	white yellowish	white yellowish	translucent	translucent	green
Particles visible inside supernatant	Al ₂ O ₃	yes	no	yes	no	no
	ZnO	yes	no	yes	yes	yes
Colour of the particles	Al ₂ O ₃	lighter brown	n/a	lighter brown	n/a	n/a
	ZnO	darker brown	n/a	darker brown	white	dark grey
Yeild	Al ₂ O ₃	59 mg (11.6%)	n/a	26.4 mg (5.2%)	n/a	n/a
	ZnO	142 mg (17.5%)	n/a	81.5 mg (10%)	352.3 mg (43.3%)	458.0 mg (56.3%)
pH	Al ₂ O ₃	2.95	n/a	n/a	n/a	4.21
	ZnO	4.04	n/a	n/a	n/a	4.10

First synthesis

During the preparation of the plant extract, the measured temperature inside the 250 ml beaker was 70°C. After the sunflower seed extract was cooled down, filtered, and centrifuged, 100 ml of sunflower solution remained (figure 3.1).

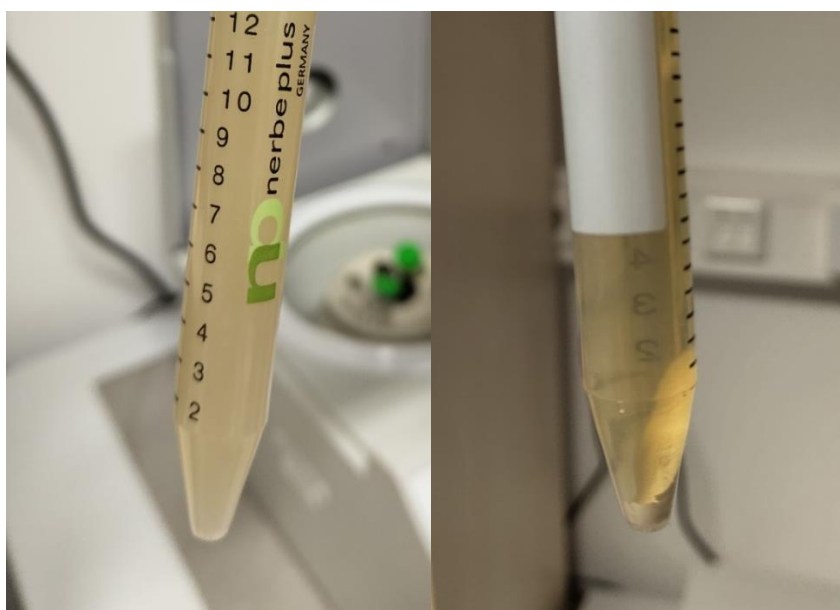


Figure 3.1. Sunflower solution before (left) and after (right) the centrifuge.

The organic molecules present in sunflower seeds act as reagents, surfactants, and stabilizers during the synthesis of the nanoparticles. The presence of surfactant on the surface of the

nanoparticles should allow them to form colloids in jet fuel thereby making a colloidal fuel. Without surfactants on their surface, the nanoparticles would fall to the bottom of the fuel due to gravity. Other surfactants can be used [2], but using green synthesis appears to be the most environmentally friendly option.

During the synthesis, the measured temperature inside the 250 ml beaker was 66°C. The aluminium solution was yellow translucent while the zinc solution appeared to be white-yellowish (figure 3.2).

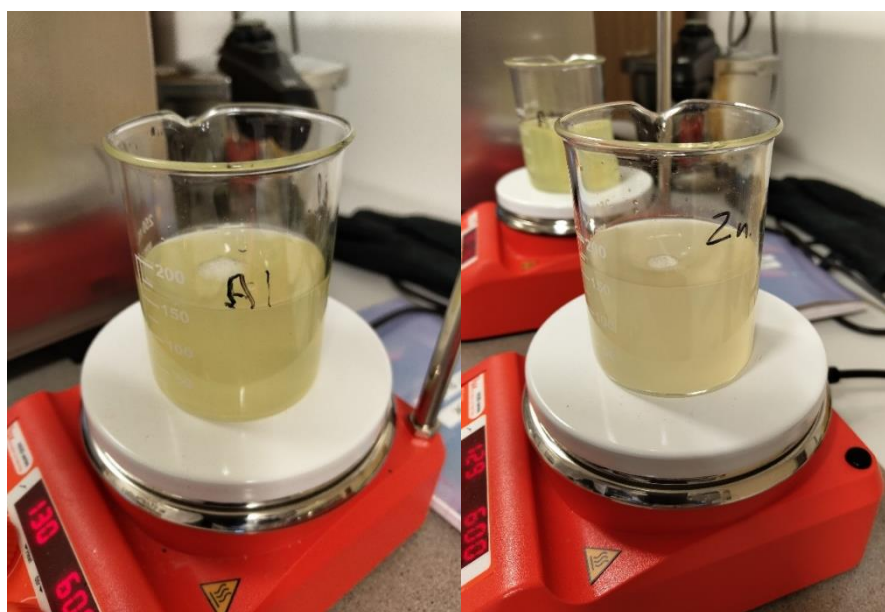


Figure 3.2. Aluminium solution (left) and zinc solution (right) while being heated and stirred.

After crushing, the resulting Al_2O_3 nanoparticles were paste-like powder with lighter brown colour and ZnO nanoparticles were a dry fine powder with a darker brown colour (figure 3.3). The pH of the Al_2O_3 and ZnO supernatants was measured at $\text{pH} = 2.95$ and $\text{pH} = 4.04$ respectively. The pH is acidic due to the utilization of nitrate as precursor.

After crushing the nanoparticles were weighed and the yield was calculated. 100% yield for Al_2O_3 and ZnO nanoparticles was calculated to be 509.8 mg and 813.9 mg respectively. The actual yield for Al_2O_3 and ZnO nanoparticles was 59 mg (11.6%) and 142 mg (17.5%) respectively. This showed a low yield, probably due to too low temperature of synthesis.



Figure 3.3. ZnO nanoparticles (top) and Al₂O₃ nanoparticles (bottom) after crushing.

Second synthesis

Covering the beaker with aluminium foil enabled to make the heating more efficient and homogeneous, and for this reason, the zinc precursor solution reached its boiling point. This is likely due to the increased heat transfer by surrounding the glass beaker with the aluminium foil (figure 3.4). Due to the boiling, a part of the water evaporated and 90 ml of ZnO solution remained at the end of synthesis.



Figure 3.4. Aluminium solution in the oven (left) and zinc solution on the heating plate (right).

After the synthesis, no visible particles could be seen inside the solutions. However, UV light confirmed the presence of the particles (figure 3.5). After centrifuging the solution inside 15 ml centrifuge test tubes, only a small quantity of particles could be seen in the bottom of the ZnO solution. There were no visible particles at the bottom of the Al₂O₃ solution. After that, 2 ml centrifuge test tubes were also used to try to extract the nanoparticles, from the solution, but it did not work, most likely due to the small size of the nanoparticles, resulting in high surface tension and low mass.

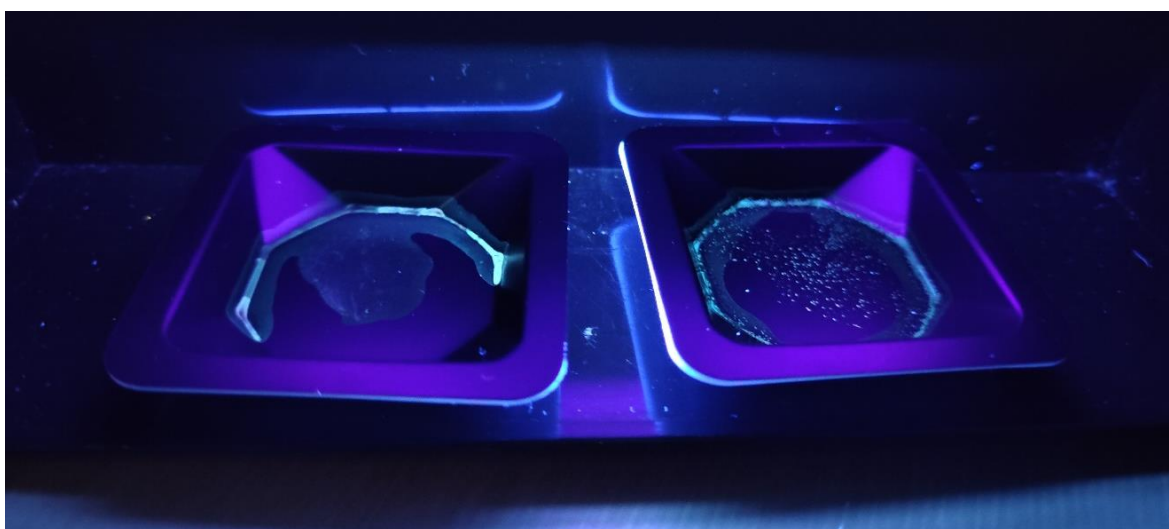


Figure 3.5. Al₂O₃ nanoparticles (left) and ZnO nanoparticles (right) under a UV light.

Third synthesis

During the third synthesis, the aluminium solution reached its boiling point and the glass beaker was covered with a glass petri dish and aluminium foil to prevent water loss (figure 3.6). Therefore, the heating plate temperature was lowered to 220°C. After the solutions had cooled, 100 ml of Al₂O₃ and 150 ml of ZnO solution remained. Both syntheses appeared successful, and particles were visible at the bottom of the beakers (figure 3.7).



Figure 3.6. Aluminium solution on the heating plate (left) and zinc solution in the oven (right).

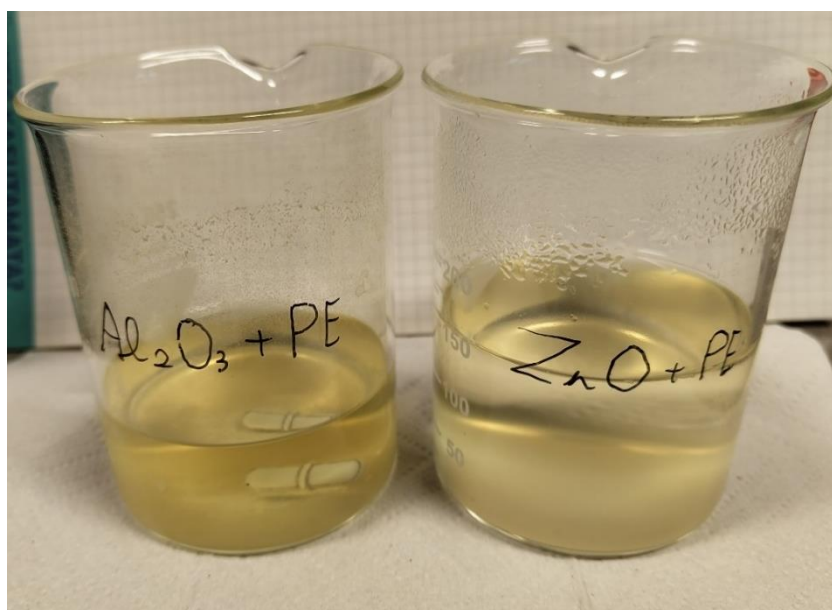


Figure 3.7. Al_2O_3 solution (left) and ZnO solution (right) after synthesis.

Both Al_2O_3 and ZnO solutions were centrifuged at 4500 rpm to avoid compressing the nanoparticles' structure. After the centrifuge, 90 ml of Al_2O_3 and 142.5 ml of ZnO supernatant remained. Supernatants were without visible solid particles. The Al_2O_3 supernatant was yellowish, while the ZnO supernatant was translucent (figure 3.8).

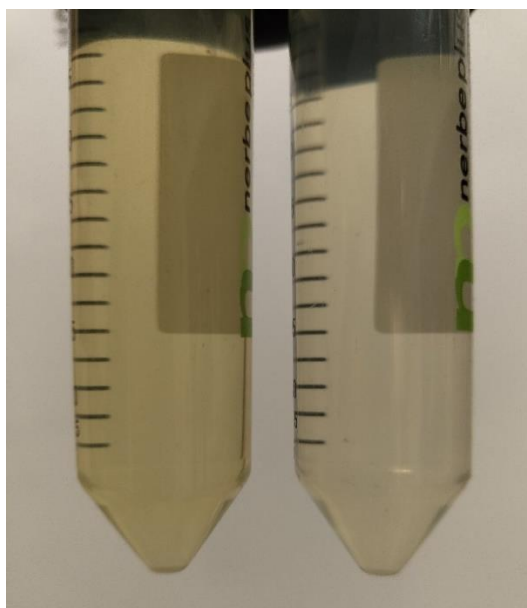


Figure 3.8. Al₂O₃ supernatant (left) and ZnO supernatant (right) after centrifuge.

After drying (figure 3.9) the nanoparticles were crushed into fine powder (figure 3.10). While crushing, the nanoparticles felt drier and were easier to crush compared to the first synthesis. After crushing the nanoparticles were weighed and the yield was calculated. 100% yield for Al₂O₃ and ZnO nanoparticles was calculated to be 509.8 mg and 813.9 mg respectively. The actual yield for Al₂O₃ and ZnO nanoparticles was 26.4 mg (5.2%) and 81.5 mg (10%) respectively.

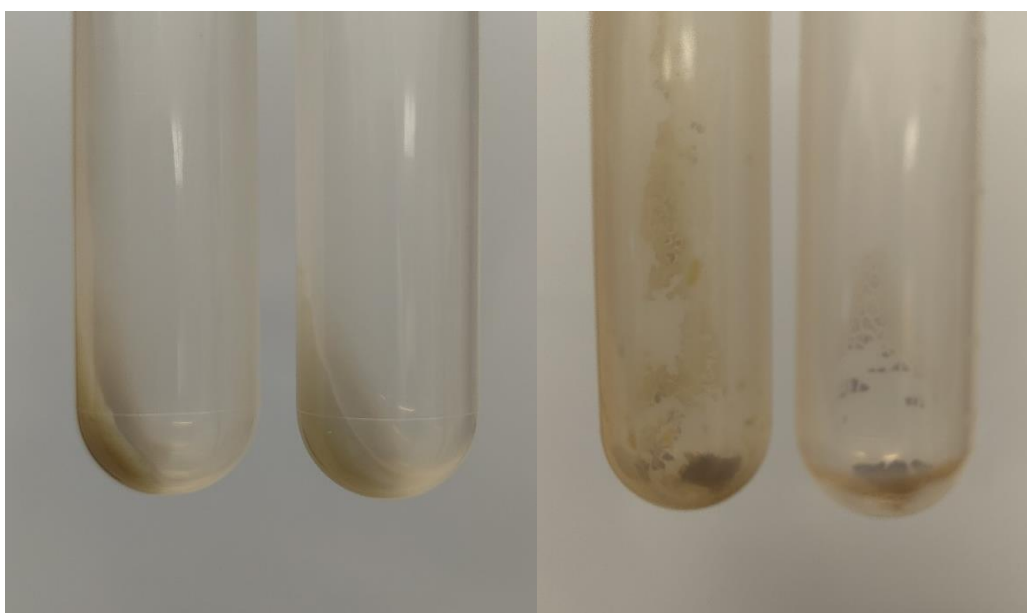


Figure 3.9. Nanoparticles after centrifuge (left) and after drying (right). The test tube with Al₂O₃ is on the right in both pictures.



Figure 3.10. Al₂O₃ nanoparticles before (left) and after (right) crushing.

Fourth synthesis

A supernatant was used to check if some precursors remained in the solution. An activator was used to enhance the reaction process. After synthesis, there were no visible particles at the bottom of the aluminium solution beaker. One reason for this might be that the Al₂O₃ nanoparticles require higher temperatures and/or longer time for the synthesis. Therefore, the aluminium solution was discarded.

However, there were some visible particles at the bottom of the zinc solution beaker. ZnO solution was centrifuged and dried (figure 3.11). After drying there was visible white powder at the bottom of the centrifuge test tubes. This means that the ZnO nanoparticles were probably not coated or only slightly coated with molecules from the plant extract. After crushing (figure 3.12) the nanoparticles were weighed and the yield was calculated. 100% yield for ZnO nanoparticles was calculated to be 813.9 mg. The actual yield was 352.3 mg (43.3%).

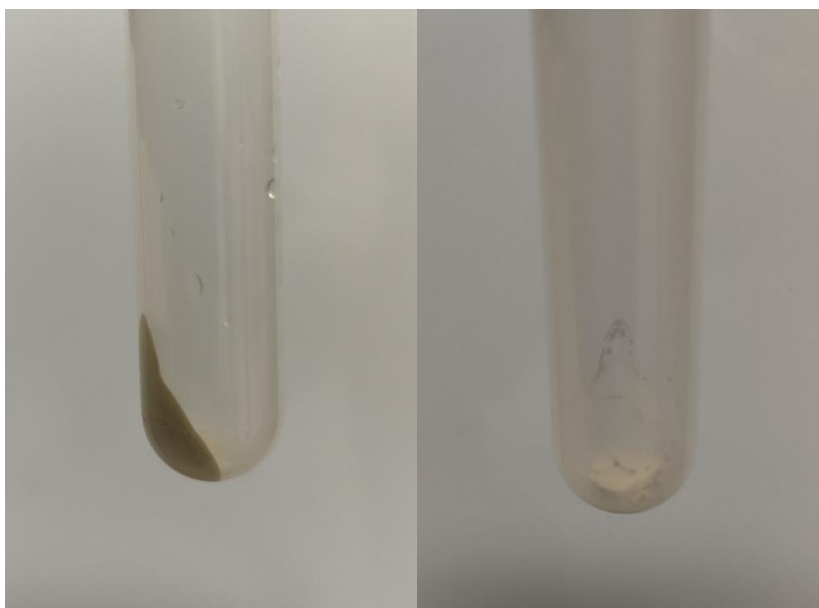


Figure 3.11. ZnO nanoparticles after centrifuge (left) and after drying (right).



Figure 3.12. ZnO nanoparticles before (left) and after (right) crushing.

Fifth synthesis

To promote the synthesis of nanoparticles at lower temperatures, an activator was used. After cooling Al_2O_3 solution remained yellow and had no visible particles at the bottom of the beaker (figure 3.13). However, the ZnO solution turned green and had a lot of visible particles at the bottom of the beaker. For both solutions, 150 ml remained after cooling. After

the centrifuge, there was no visible separation for Al_2O_3 nanoparticles. Therefore, separation of the Al_2O_3 nanoparticles could not be performed. However, for the ZnO, there were a lot of green nanoparticles at the bottom of the centrifuge test tubes (figure 3.14). After the centrifuge, 131 ml of ZnO supernatant remained. The pH of the Al_2O_3 and ZnO supernatants was measured at $\text{pH} = 4.21$ and $\text{pH} = 4.10$ respectively.

After crushing (figure 3.15) the nanoparticles were weighed and the yield was calculated. 100% yield for ZnO nanoparticles was calculated to be 813.9 mg. The actual yield was 458.0 mg (56.3%).

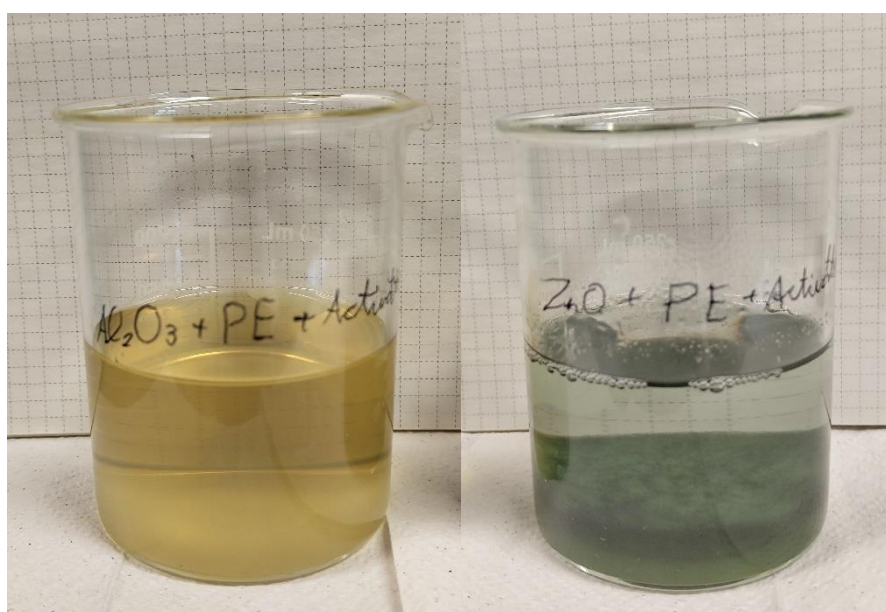


Figure 3.13. Al_2O_3 solution (left) and ZnO solution (right) after synthesis.

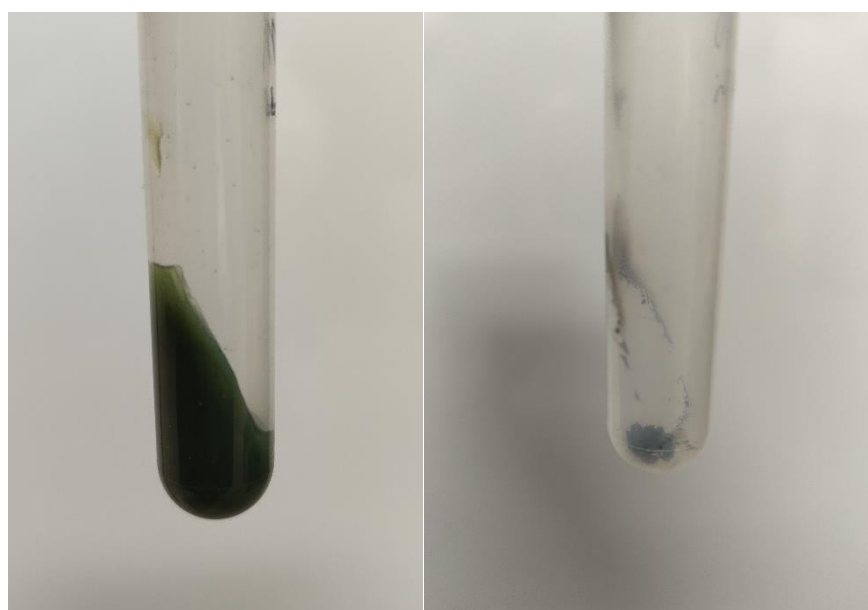


Figure 3.14. ZnO nanoparticles after centrifuge (left) and after drying (right).



Figure 3.15. ZnO nanoparticles before (left) and after (right) crushing.

3.1.2. Results of UV-vis spectrophotometer analyses

First synthesis

During the preparation for the UV-vis spectrophotometer analyses, Al_2O_3 nanoparticles seemed to disperse easily in isopropanol, however, the dispersion of ZnO nanoparticles was more complicated and it was possible to see the nanoparticles falling into the bottom of the solution (figure 3.16). This experiment showed that ZnO nanoparticles are probably bigger or agglomerated, and do not form a colloidal solution in isopropanol. From the absorbance using isopropanol as a baseline Tauc Plots were calculated for both samples (figure 3.17).

The band gap of Al_2O_3 and ZnO solutions were measured at 3.56 eV and 3.46 eV respectively. The band gap for Al_2O_3 is similar to that of Al_2O_3 thin films [30]. However, for ZnO, the band gap is similar to the ZnO nanoparticle band gap found in previous research [31].

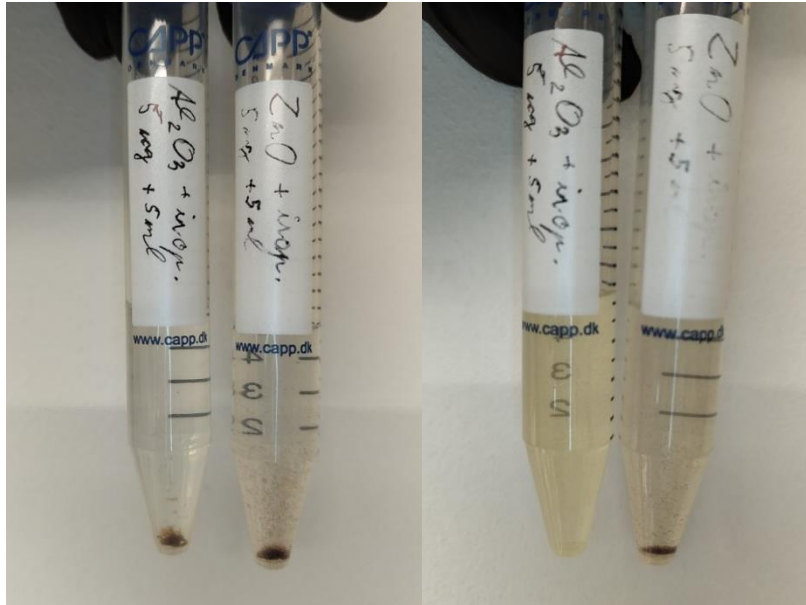


Figure 3.16. Nanoparticles before (left) and after (right) ultrasonic cleaner. Al_2O_3 nanoparticles are on the left and ZnO nanoparticles are on the right in both pictures.

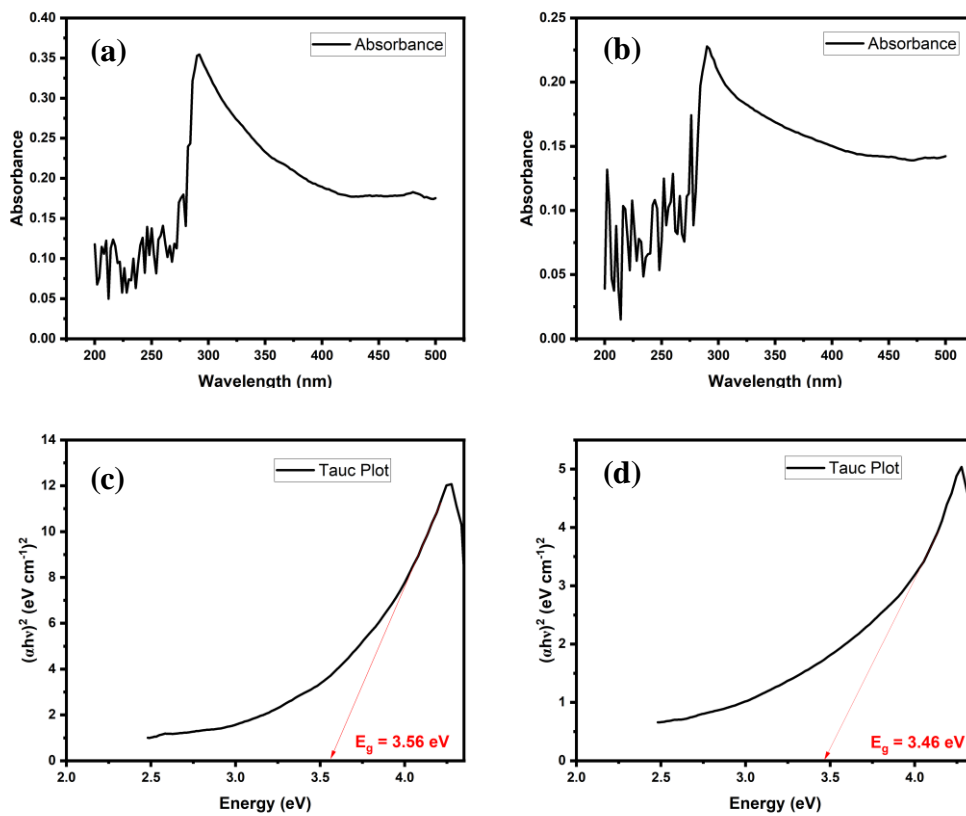


Figure 3.17. Absorbance (isopropanol as a baseline) of Al_2O_3 (a) and ZnO (b) and Tauc Plot of Al_2O_3 (c) and ZnO (d).

After mixing Jet A-1 with 40 ppm nanoparticles, UV-vis spectrophotometer analyses were performed. From the absorbance using Jet A-1 as a baseline Tauc Plots were calculated for both samples (figure 3.18).

The band gap of Al_2O_3 was measured at 3.72 eV. However, it was not possible to measure the band gap of the ZnO due to the excessive noise in the Tauc Plot.

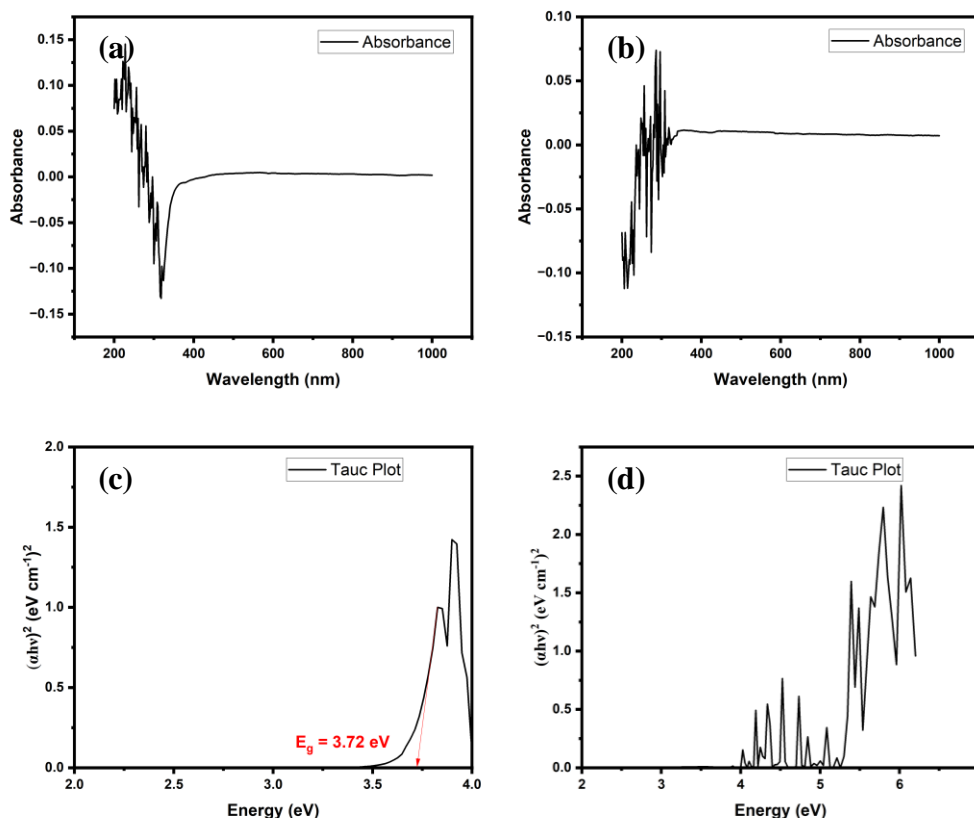


Figure 3.18. Absorbance (Jet A-1 as a baseline) of 40 ppm Al_2O_3 nanoparticles solution (a) and 40 ppm ZnO 40 nanoparticles solution (b) and Tauc Plot of 40 ppm Al_2O_3 nanoparticles solution (c) and 40 ppm ZnO nanoparticles solution (d).

Jet A-1 was also mixed with 100 ppm of ZnO nanoparticles, and UV-vis spectrophotometer analyses were performed. From the absorbance using Jet A-1 as a baseline Tauc Plots were calculated (figure 3.19). Similarly to the 40 ppm concentration, it was not possible to measure the band gap from the 100 ppm ZnO nanoparticle Jet A-1 mix.

UV-vis spectrophotometer analyses did not confirm the presence of nanoparticles. This is because Jet A-1 fuel absorbs at the same wavelength as the nanoparticles. The quantity of nanoparticles added is relatively small (40-100 ppm) compared to the amount of fuel.

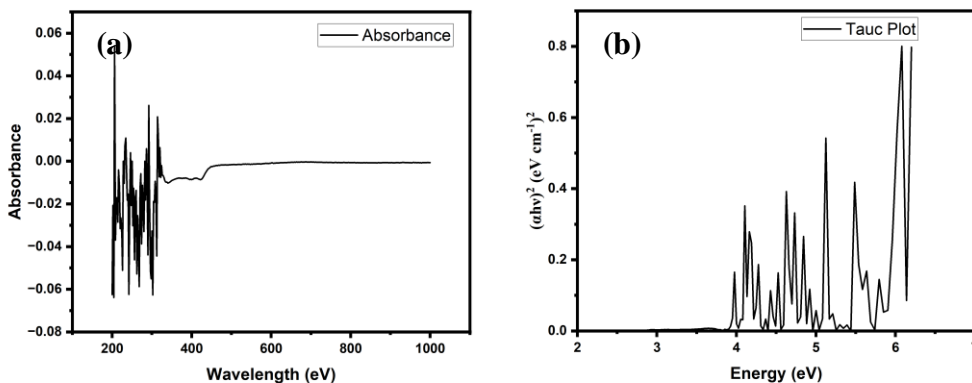


Figure 3.19. Absorbance (Jet A-1 as a baseline) (a) and Tauc Plot (b) of 100 ppm ZnO nanoparticles solution.

Third synthesis

UV-vis spectrophotometer analyses were performed for both Al₂O₃ and ZnO nanoparticles. For that 5 ml of isopropanol with 5 mg of nanoparticles was used. From the absorbance using isopropanol as a baseline Tauc Plots were calculated for both samples (figure 3.20).

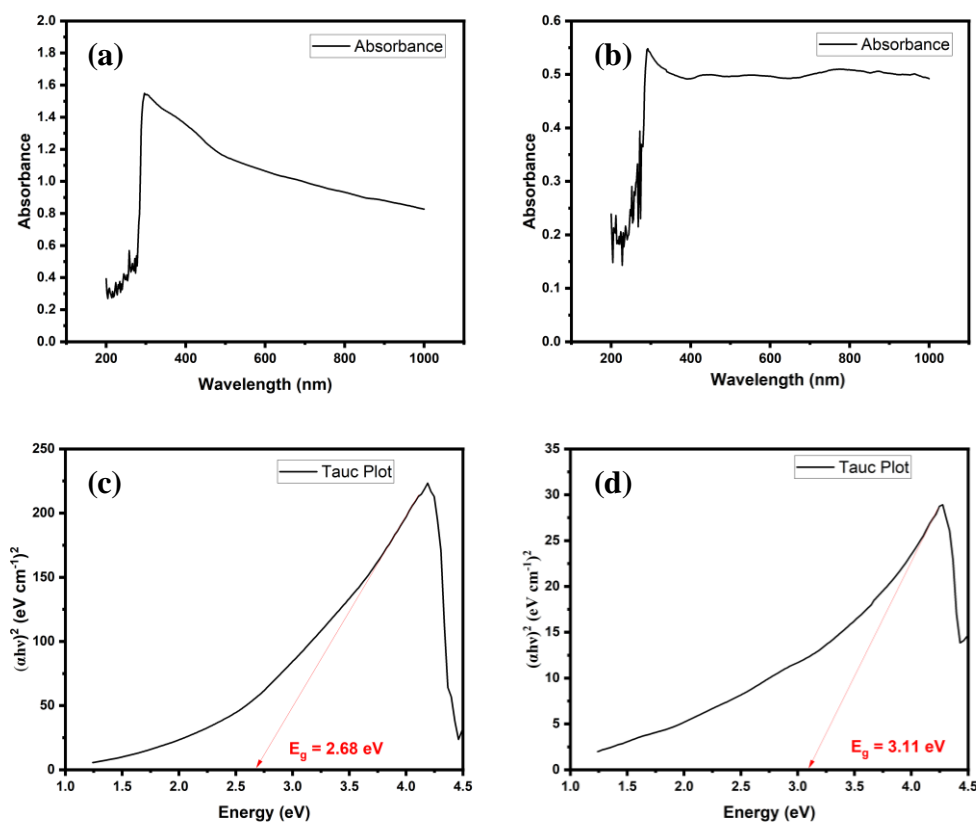


Figure 3.20. Absorbance (isopropanol as a baseline) of Al₂O₃ nanoparticles solution (a) and

ZnO nanoparticles solution (b) and Tauc Plot (isopropanol as a baseline) of Al₂O₃ nanoparticles solution (c) and ZnO nanoparticles solution (d).

The band gap of Al₂O₃ and ZnO solutions were measured at 2.68 eV and 3.11 eV respectively. The band gap for Al₂O₃ is smaller than can be found in the literature [30]. However, for ZnO, the band gap is similar to previous research [31].

Fifth synthesis

UV-vis spectrophotometer analyses were performed for ZnO nanoparticles. For that 5 ml of isopropanol with 5 mg of nanoparticles was used. From the absorbance using isopropanol as a baseline Tauc Plots were calculated (figure 3.21). The band gap of ZnO solution was measured at 2.89 eV which is smaller than on the previous syntheses.

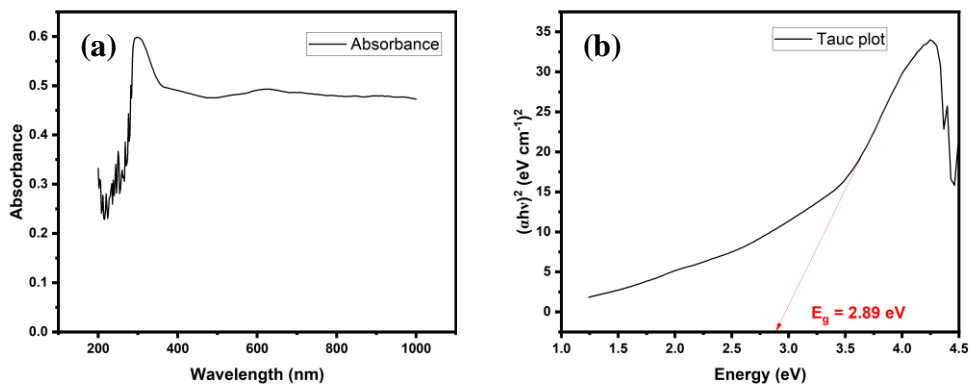


Figure 3.21. Absorbance (isopropanol as a baseline) (a) and Tauc Plot (b) of 100 ppm ZnO nanoparticles solution.

3.1.3. Temperature calibration of the heating plate temperature

During the heating plate temperature experiment, an interval of approximately 15 minutes was applied between each temperature increase, to let the temperature inside the beaker stabilise. Due to the evaporation, at the end of the experiment, 80 ml of distilled water remained inside the beaker. When the heating plate was set to 130°C, the temperature inside the beaker was measured at 66°C. While the heating plate was set to 280°C, the temperature inside the beaker was measured at 94°C (figure 3.22).

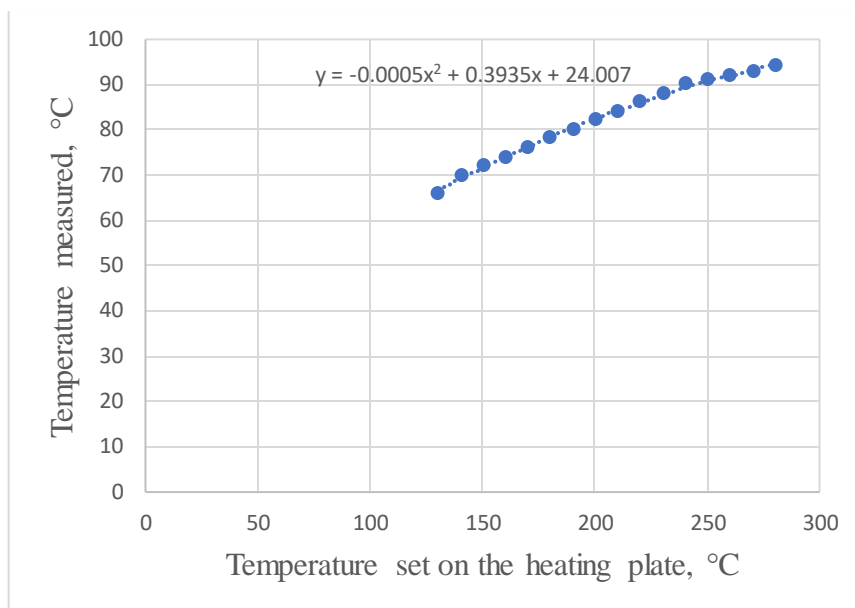


Figure 3.22. Temperature set on the heating plate in correlation with the temperature measured inside of the 250 ml glass beaker.

3.1.4. FTIR analyses results

From the Al_2O_3 FTIR analyses (figure 3.23), the presence of NO_3 molecules can be seen between 1322 and 1552 cm^{-1} . Organic compounds can be seen at different wavenumbers. Compared to the ZnO samples, the Al_2O_3 samples contain both more NO_3 and organic molecules. One possibility for that is the overall lower yield of the Al_2O_3 synthesis. Therefore, the resulting substance has fewer Al_2O_3 nanoparticles and more of the other compounds.

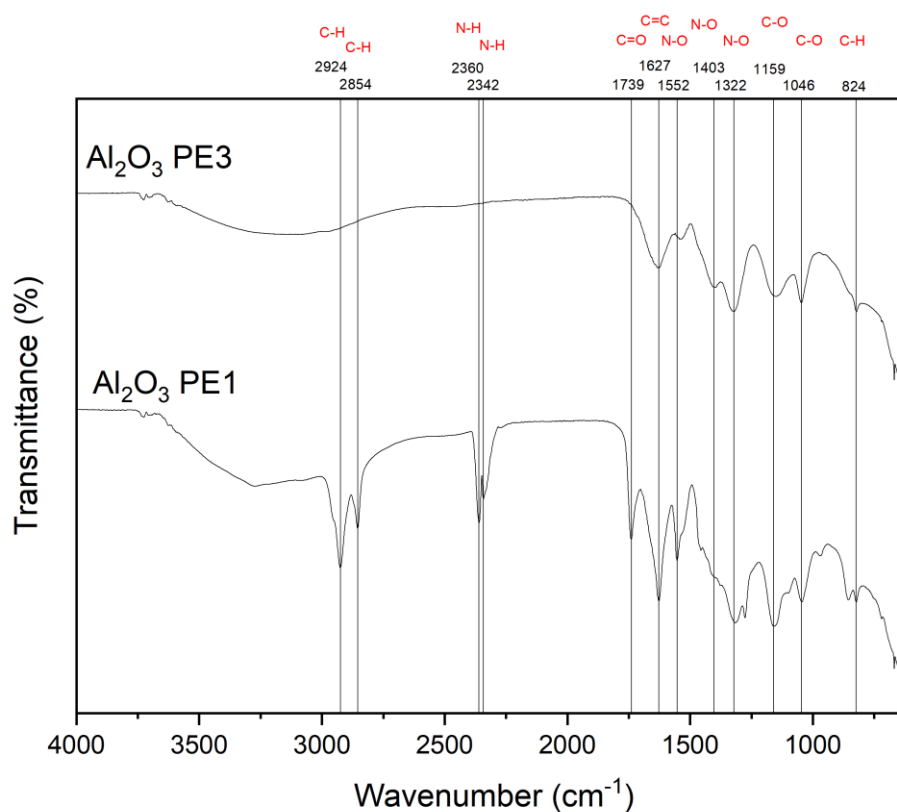


Figure 3.23. FTIR analyses results of Al₂O₃ nanoparticles.

From the ZnO FTIR analyses (figure 3.24), the presence of NO_x molecules can be seen between 1311 and 1540 cm⁻¹. This means that by adding nanoparticles to the fuel, increased NO_x emissions can be expected. However, for the ZnO nanoparticles from the fifth synthesis, NO_x molecule quantity seems to be considerably lower than in nanoparticles from the third and fourth synthesis. Therefore, by adding a precursor to the synthesis, yield can be increased and resulting NO_x emissions can be reduced. The presence of aromatic disubstituted benzene molecules can be seen between 807 and 1000 cm⁻¹. The presence of organic compounds on the surface of the nanoparticles is important, as they act as surfactants, therefore allowing the formation of colloidal fuel.

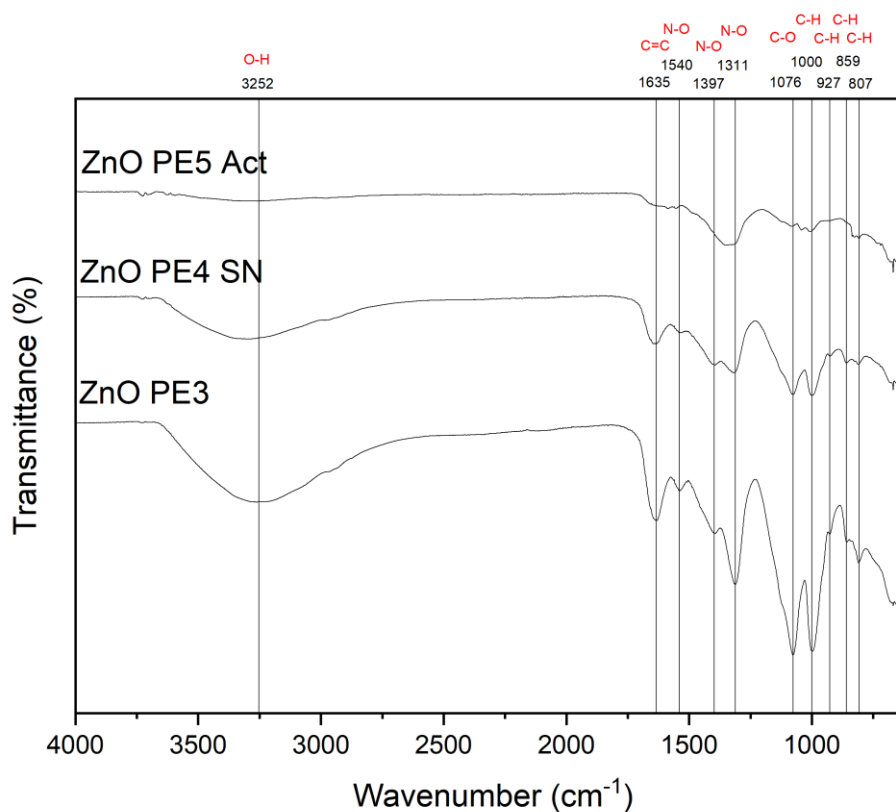


Figure 3.24. FTIR analyses results of ZnO nanoparticles.

3.1.5. SEM analyses results

From the SEM images (figure 3.25), we can observe the morphology of ZnO nanoparticles. The ZnO PE3 sample shows no geometrical shape, probably lacking distinct crystalline features. In contrast, the ZnO PE4 SN sample exhibits well-defined edges and facets, which could indicate crystalline nanoparticle with hexagonal Wurtzite structure. The ZnO PE5 Act sample, while also demonstrating similar characteristics, exhibit different shapes and less defined edges and facets compared to the ZnO PE4 SN sample, suggesting a possible lower degree of crystallinity or slightly different growth.

From the energy-dispersive X-ray spectroscopy (EDS) scan we can see that PE3 contains ZnO and phosphorous (from sunflower seed). PE4 SN contains only ZnO, no plant extract is attached (confirmed by the colour) and PE5 Act contains ZnO and sodium with traces of phosphorous.

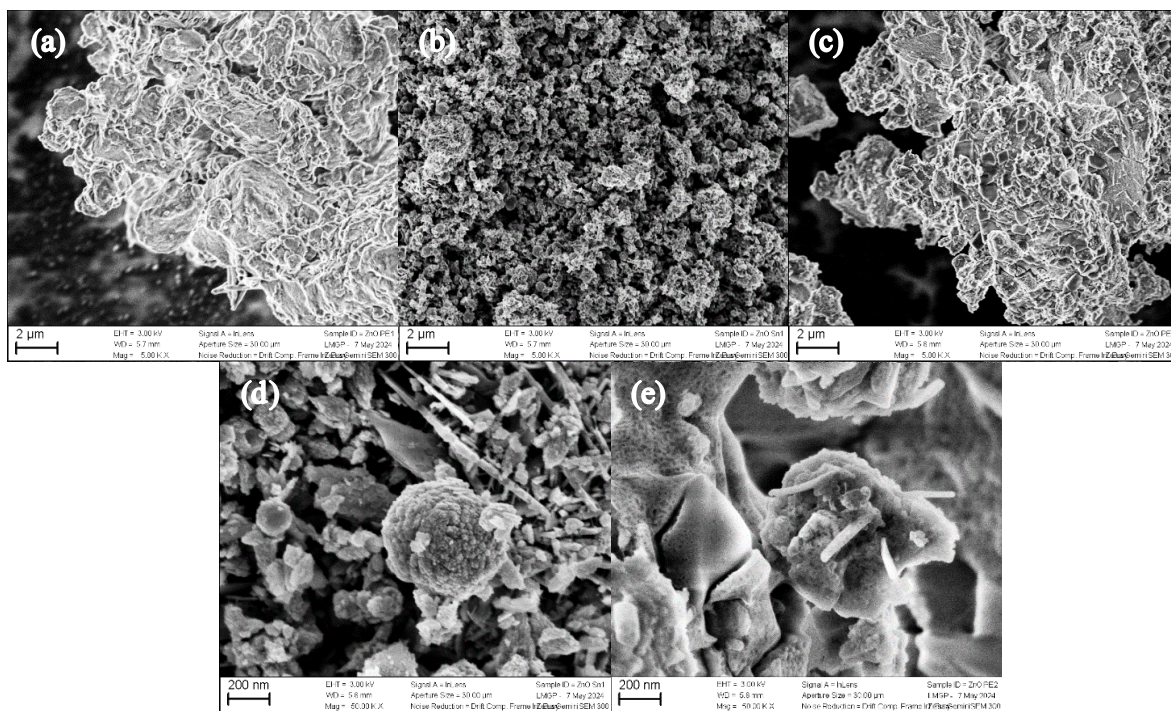


Figure 3.25. SEM 2 μm images of ZnO PE3 (a), ZnO PE4 SN (b), ZnO PE5 Act (c) and SEM 200 nm images of ZnO PE4 SN (d) and ZnO PE5 Act (e).

3.1.6. XRD analyses results

The XRD study (figure 3.26) confirmed that the ZnO PE3 sample is amorphous, indicating that it lacks a long-range crystalline order. In contrast, the ZnO PE4 SN sample was found to possess a hexagonal wurtzite-analogous ($P6_3mc$) crystal structure, which is a stable structure of ZnO. By applying the Scherrer method [32] to the 100 and 002 reflections (table 3.2) the crystallite sizes for the ZnO PE4 SN sample were estimated to be approximately 18 nm and 31 nm, respectively. Furthermore, the average crystallite size for the ZnO PE4 SN sample was calculated using the Scherrer equation, resulting in an estimated size of around 24.7 nm. This indicates a consistent crystallinity within the sample, albeit with some variation in crystallite sizes. The (002) plane shows the largest crystallites, indicating higher size in this direction, but it must be confirmed by transmission electron microscope study.

Table 3.2. ZnO PE4 SN X-ray diffraction peak values used for Scherrer calculation measurements

<i>hkl</i>	100	002	101	102	110	103	112
2θ (deg)	31.79	34.44	36.28	47.55	56.60	62.84	68.03
fwhm (deg)	0.450	0.269	0.469	0.605	0.581	0.669	1.982
Ø (nm)	18.35	30.95	17.81	14.35	15.52	13.92	4.835

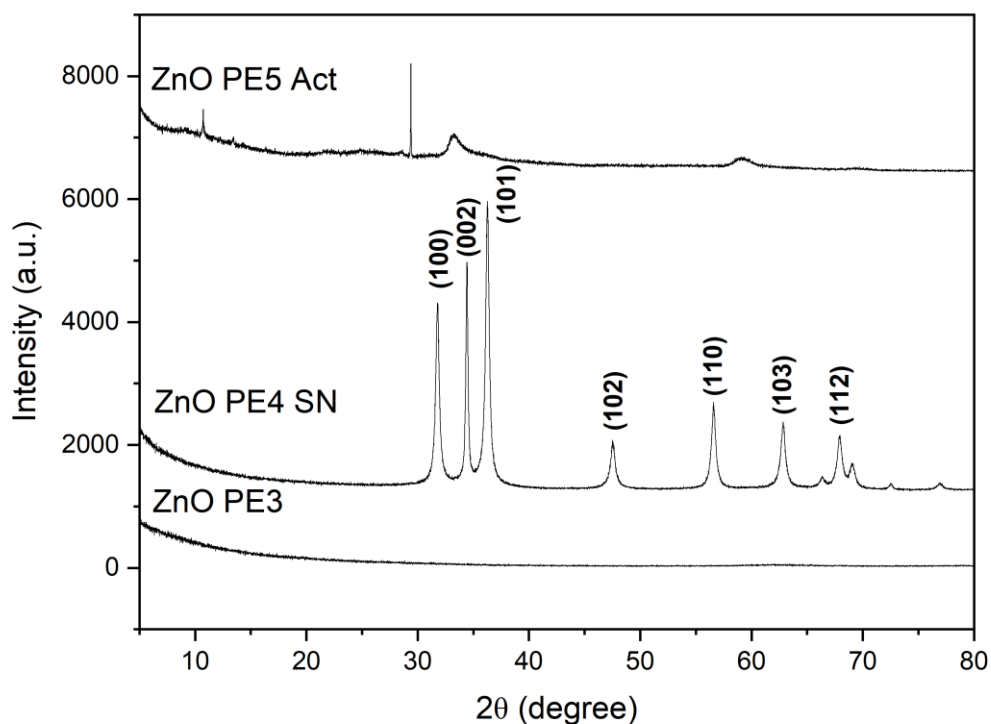


Figure 3.26. XRD analysis results of ZnO nanoparticles.

3.1.7. Fuel analyses results

The analyses of Jet A-1 fuel samples (table 3.3), one without nanoparticles and the other containing 100 ppm of ZnO nanoparticles (first synthesis), revealed several noteworthy observations. Firstly, the cetane index, an indicator of ignition quality, remained consistent at 46.1 for both samples, indicating negligible influence of ZnO nanoparticles on this parameter. However, a significant reduction in flash point was observed in the nanoparticle-containing sample (30.0°C) compared to the pure Jet A-1 (45.0°C), suggesting enhanced flammability with nanoparticle inclusion. The significant reduction in flash point observed in the nanoparticle-containing jet fuel sample may enhance cold weather performance and

combustion efficiency, potentially leading to improved operational effectiveness. However, these performance benefits come with increased safety risks and potential regulatory compliance issues that must be carefully managed. Density measurements at 15°C showed minimal disparity between the two samples, with values of 797.9 kg/m³ and 798.0 kg/m³ for pure Jet A-1 and Jet A-1 with ZnO nanoparticles, respectively, implying marginal impact on fuel density due to nanoparticle incorporation.

Remarkably, a substantial decrease in initial boiling point was recorded in the Jet A-1 with ZnO nanoparticles (94.3°C) compared to the pure counterpart (164.4°C), indicating a lowered threshold for fuel vaporization with nanoparticle addition. Conversely, the final boiling point exhibited minimal deviation between the samples, with values of 242.5°C and 243.0°C for pure Jet A-1 and Jet A-1 with ZnO nanoparticles, respectively, indicating comparable endpoint temperatures of the distillation process.

The considerable decrease in the initial boiling point of Jet A-1 with ZnO nanoparticles compared to pure fuel highlights promising enhancements in fuel performance. Similarly, the significant drop in flash point offers potential benefits for fuel efficiency and cold weather operability. These results inspire further investigation to fully understand the underlying mechanisms driving these changes. Thus, comprehensive validation through additional experiments and complementary analytical techniques will confirm the reliability and reproducibility of these findings.

Table 3.3. Result of the fuel analyses for Jet A-1 and Jet A-1 with 100 ppm of ZnO

Properties	Temperature or volume percentage	
	Jet A-1	Jet A-1 + 100 ppm ZnO
Cetane index	46.1	46.1
Flash point, °C	45.0	30.0
Density (15 °C), kg/m ³	797.9	798.0
Initial boiling point, °C	164.4	94.3
Final boiling point, °C	242.5	243.0
5 % volume distillate, °C	175.7	175.9
10 % volume distillate, °C	177.9	178.6
20 % volume distillate, °C	182.2	182.5
30 % volume distillate, °C	186.7	187.2
40 % volume distillate, °C	191.4	191.9
50 % volume distillate, °C	196.5	197.3
60 % volume distillate, °C	202.6	202.7
70 % volume distillate, °C	209.5	210.0
80 % volume distillate, °C	217.7	218.2
90 % volume distillate, °C	228.1	228.2
95 % volume distillate, °C	236.0	236.8

3.2. Engine tests results

After five synthesis attempts, zinc oxide was chosen for subsequent fuel and engine testing due to the poor yield and synthesis challenges associated with aluminium oxide. For the engine trials, ZnO PE 4 SN (fourth synthesis) nanoparticles were selected, as ZnO PE 5 Act (fifth synthesis) nanoparticles did not mix properly with Jet A-1. This poor mixing is likely due to the hydrophilic nature of ZnO PE 5 Act nanoparticles. In contrast, ZnO PE 4 SN nanoparticles exhibited favourable mixing properties with Jet A-1 and did not display any discernible hydrophilic traits.

During the engine testing, conducted with the pure fuel tests performed initially followed by the nanoparticle fuel tests, some challenges with the testing equipment, including incorrect or missing sensor readings, were encountered. However, despite these issues, each test ensured the engine reached its operating temperature promptly, with sufficient cooldown intervals between tests. Specifically, two control tests were conducted with pure Jet A-1, followed by two tests with the NAF. The results from the engine tests were averaged for both the pure fuel and the fuel with additives (table 3.4).

Table 3.4. The result of the engine tests

Properties	Reading from the test stand	
	Jet A-1	Jet A-1 + 100 ppm ZnO
Inlet airspeed, m/s	56.3	57.2
Exhaust airspeed, m/s	34.7	37.15
Inlet air temperature, °C	19.64	20.75
Exhaust air temperature, °C	459.41	462.51
Inlet air pressure, kPa	94.6	95.4
Exhaust air pressure, kPa	96.0	97.25
Inlet air mass, g/s	875	880
Exhaust air mass, g/s	1357	1435
Exhaust CO, %	0.105	0.112
Exhaust CO ₂ , %	2.53	2.56
Exhaust HC, ppm	34	49
Exhaust NO _x , ppm	10	12
Exhaust O, %	17.38	17.24

The results indicate that the addition of ZnO slightly increased the inlet airspeed from 56.3 m/s to 57.2 m/s and the exhaust airspeed from 34.7 m/s to 37.15 m/s. This suggests that the fuel mixture with ZnO might improve the engine's performance by enhancing airspeed.

Regarding air temperature, the inlet temperature rose slightly from 19.64°C to 20.75°C, while the exhaust temperature increased from 459.41°C to 462.51°C. These changes suggest

that the combustion process is slightly more efficient with the ZnO additive, leading to higher temperatures.

Air pressure readings also showed minor increases with ZnO. The inlet air pressure increased from 94.6 kPa to 95.4 kPa, and the exhaust air pressure rose from 96.0 kPa to 97.25 kPa. This indicates a more efficient compression and combustion process within the engine.

The air mass flow data showed an increase in the inlet air mass from 875 g/s to 880 g/s and a more significant increase in the exhaust air mass from 1357 g/s to 1435 g/s. The substantial rise in exhaust air mass flow suggests that the engine processes a larger volume of air, potentially translating to increased thrust or power output.

However, the exhaust emissions data present some concerns. CO emissions slightly increased from 0.105% to 0.112%, and CO₂ emissions rose from 2.53% to 2.56%. Hydrocarbon emissions increased notably from 34 ppm to 49 ppm, representing a 44.1% increase. NO_x emissions went up from 10 ppm to 12 ppm, which is a 20% increase. The percentage of oxygen in the exhaust decreased slightly from 17.38% to 17.24%. These changes indicate that while ZnO improves certain performance metrics, it also results in higher emissions of pollutants like CO, HC, and NO_x, suggesting incomplete combustion and increased formation of nitrogen oxides. The increased NO_x emissions are likely due to the presence of the NO₃ molecules from the Zn precursor. These are visible in FTIR analyses, supporting the higher release of nitrogen oxides during combustion. Additional rinsing of the nanoparticles could potentially reduce the HC emissions by removing residual synthesis by-products.

The findings from the engine tests, which indicate increased emissions of CO, HC, and NO_x with the addition of 100 ppm ZnO nanoparticles to Jet A-1 fuel, appear to contradict the expectations derived from existing literature. Previous studies and theoretical predictions would suggest that the inclusion of ZnO nanoparticles in the fuel would lead to reduced emissions rather than elevated levels. The literature often suggests that nanoparticles can act as catalysts, promoting more complete combustion and thereby reducing emissions of harmful pollutants. However, the observed increase in emissions in the current study implies a different interaction between the nanoparticles and the combustion process than what was anticipated. This unexpected outcome highlights the complexity of engine performance and emissions dynamics and underscores the importance of empirical testing to validate theoretical predictions. Further investigation is needed to understand the mechanisms behind

these divergent results and to optimize the use of nanoparticles as fuel additives for emission reduction purposes.

In conclusion, incorporating 100 ppm ZnO into Jet A-1 fuel demonstrates significant enhancements in engine performance, including increased airspeed, improved thermal efficiency, and enhanced air mass flow. This promising improvement underscores the potential of ZnO as a valuable fuel additive. However, the synthesis method plays a pivotal role, as higher emissions are observed, likely stemming from the synthesis process itself. This emphasises the importance of refining and optimising the synthesis approach to enable enhanced combustion without compromising environmental standards. While ZnO holds tremendous promise for boosting performance, addressing its environmental impact through synthesis refinement is crucial for its widespread adoption in aviation. Additionally, the effects of nanoparticles at high altitudes, where air temperature is much lower, should be investigated to fully understand their impact under different operating conditions.

SUMMARY AND CONCLUSION

The primary aim of this master's thesis was to investigate the impact of nanoparticles on jet fuel. Based on a review of the literature, testing was conducted using aluminium oxide and zinc oxide nanoparticles synthesized via a green synthesis approach. The green synthesis method was selected for its environmental compatibility and precedent in previous studies. Sunflower seeds were chosen as the precursor due to their high oil content that can facilitate homogeneous dispersion of nanoparticles within the jet fuel, resulting in a final colloidal solution.

The literature review shows that many studies demonstrate positive outcomes from tests involving diesel fuel and nanoparticle additives, encompassing diverse nanoparticle types and concentrations across different fuel variants. Aluminium oxide and zinc oxide were chosen for nanoparticle synthesis, with aluminium oxide selected due to its extensive prior research and zinc oxide chosen for its environmental friendliness and prior laboratory experimentation.

After five syntheses, zinc oxide was selected for subsequent fuel and engine testing, as aluminium oxide exhibited poor yield till now and synthesis challenges compared to zinc oxide. Physical and chemical tests were conducted on both Jet A-1 fuels to ensure accuracy, encompassing distillation characteristics, flash point, and density. The analysis of fuel samples revealed several noteworthy observations. Despite consistent cetane index values indicating minimal influence of nanoparticles on ignition quality, a significant reduction in flash point was observed in the nanoparticle-containing sample, suggesting enhanced flammability. Density measurements showed minimal disparity between the samples, implying a marginal impact on fuel density due to nanoparticle incorporation.

To assess the effects of 100 ppm ZnO nanoparticles in Jet A-1 fuel, engine tests measured various parameters including airspeed, temperature, pressure, and exhaust emissions. The results showed that ZnO nanoparticles improved engine performance, as indicated by increased airspeeds, temperatures, and pressures.

However, the addition of ZnO led to higher emissions: CO increased from 0.105% to 0.112%, CO₂ rose from 2.53% to 2.56%, hydrocarbons increased from 34 ppm to 49 ppm (a 44.1% increase), and NO_x emissions went up from 10 ppm to 12 ppm (a 20% increase). The

increased NO_x emissions are likely due to the presence of the NO₃ molecules from the zinc precursor used for the synthesis as observed in FTIR analyses. The rise in HC emissions may also be attributed to the synthesis process, and additional rinsing of the nanoparticles could potentially mitigate this increase.

Due to this, findings from the engine tests do not align with the results typically reported in the literature. According to previous studies, the incorporation of ZnO nanoparticles into fuel formulations is often associated with reductions in emissions of pollutants such as CO, HC, and NO_x. This suggests that the effects of ZnO nanoparticles on combustion processes may vary depending on specific engine configurations, operating conditions, fuel compositions, and precursors used for the synthesis. Further investigation is needed to understand the underlying mechanisms responsible for the observed increase in emissions.

In conclusion, while the addition of 100 ppm ZnO to Jet A-1 fuel enhances engine performance, it could also result in higher emissions of pollutants, necessitating careful consideration of its environmental impact and potential measures to address these emissions. More research is needed into the synthesis of ZnO nanoparticles and the creation of stable colloidal solutions of Jet A-1 and nanoparticles that remain stable over extended periods. Improved nanoparticle coating and grinding techniques should be explored to achieve this stability. Additionally, findings from this research should be confirmed through further fuel and engine tests, and different concentrations of nanoparticle additives should be tested to optimise performance and emissions. Research on the impact of nanoparticles on the fuel filter is also essential to ensure the long-term viability of these additives in practical applications.

LITERATURE

- [1] About Gas Turbines – Principle of gas turbine operation. – *Kawasaki*. [on-line] https://global.kawasaki.com/en/energy/equipment/gas_turbines/outline.html (15.02.2023).
- [2] **Khan, S., Dewang, Y., Raghuvanshi, J., Shrivastava, A., Sharma, V.** (2020). Nanoparticles as fuel additive for improving performance and reducing exhaust emissions of internal combustion engines. - *Taylor & Francis Online. International Journal of Environmental Analytical Chemistry*. Volume 102, Issue 2. [on-line] <https://www.tandfonline.com/doi/full/10.1080/03067319.2020.1722810> (15.02.2023).
- [3] **Küçükosman, R., Yontar, A, A., Ocakoglu, K.** (2022). Nanoparticle additive fuels: Atomization, combustion and fuel characteristics. – *Elsevier. Journal of Analytical and Applied Pyrolysis*. Volume 165. [on-line] <https://www.sciencedirect.com/science/article/abs/pii/S0165237022001450?via%3Dihub> (15.02.2023).
- [4] **Yusof, S, N, A., Sidik, N, A, C., Asako, Y., Mohd, W., Japar, A, A., Mohamed, S, B., Muhammad, N, M.** (2020). A comprehensive review of the influences of nanoparticles as a fuel additive in an internal combustion engine (ICE). – *De Gruyter*. [on-line] <https://www.degruyter.com/document/doi/10.1515/ntrev-2020-0104/html?lang=en> (15.02.2023).
- [5] **Petratškov, S.** (2021). The Impact of ZnO Nano-additives in Diesel Fuel on the Efficiency Parameters and Exhaust Gas Emission of a Diesel Engine. – *EMU DSpace*. [on-line] <https://dspace.emu.ee/xmlui/handle/10492/6904?show=full> (15.02.2023).
- [6] **Soudagar, M, E, M., Banapurmath, N, R., Afzal, A., Hossain, N., Abbas, M, M., Haniffa, M, A, C, M., Naik, B., Ahmed, W., Nizamuddin, S., Mubarak, N, M.** (2020). Study of diesel engine characteristics by adding nanosized zinc oxide and diethyl ether additives in Mahua biodiesel–diesel fuel blend. – *Nature. Scientific Reports*. Volume 10. [on-line] <https://www.nature.com/articles/s41598-020-72150-z> (15.02.2023).
- [7] **Ferrão, I, A, S., Mendes, M, A, A., Moita, A, S, O, H., Silva, A, R, R.** (2022). The Addition of Particles to an Alternative Jet Fuel. – *MDPI. Fuels*. Volume 3, Issue 2. [on-line] <https://www.mdpi.com/2673-3994/3/2/12> (15.02.2023).
- [8] **Guerieri, P, M., Jacob, R, J., DeLisio, J, B., Rehwoldt, M, C., Zachariah, M, R.** (2017). Stabilized microparticle aggregates of oxygen-containing nanoparticles in kerosene for enhanced droplet combustion. – *Elsevier. Combustion and Flame*. Volume 187. [on-line]

- <https://www.sciencedirect.com/science/article/abs/pii/S0010218017303231?via%3Dihub>
(15.02.2023).
- [9] **Kannaiyan, K., AIDosari, A., Sadr, R.** (2020). Effects of nanoscale fuel additives on properties and non-reacting spray performance of alternative, conventional and blended jet fuels at elevated ambient conditions. – *Elsevier. Fuel Processing Technology*. Volume 208. [on-line] <https://www.sciencedirect.com/science/article/abs/pii/S0378382020303180?via%3Dihub>
(15.02.2023).
- [10] **Sonawane, S., Patankar, K., Fogla, A., Puranik, B., Bhandarkar, U., Kumar, S, S.** (2011). An experimental investigation of thermo-physical properties and heat transfer performance of Al₂O₃-Aviation Turbine Fuel nanofluids. – *Elsevier. Applied Thermal Engineering*. Volume 31. [on-line] <https://www.sciencedirect.com/science/article/abs/pii/S1359431111002614?via%3Dihub>
(15.02.2023).
- [11] Nanoparticle production – How nanoparticles are made. – *Nanowerk*. [on-line] https://www.nanowerk.com/how_nanoparticles_are_made.php (15.02.2023).
- [12] **Balachandran, A., Sreenilayam, S, P., Madanan, K., Thomas, S., Brabazon, D.** (2022). Nanoparticle production via laser ablation synthesis in solution method and printed electronic application - A brief review. – *Elsevier. Results in Engineering*. Volume 16. [on-line] <https://www.sciencedirect.com/science/article/pii/S2590123022003164?via%3Dihub>
(15.02.2023).
- [13] **Jadoun, S., Arif, R., Jangid, N, K., Meena, R, K.** (2021). Green synthesis of nanoparticles using plant extracts: a review. – *Springer Link. Environmental Chemistry Letters*. Volume 19. [on-line] <https://link.springer.com/article/10.1007/s10311-020-01074-x> (15.02.2023).
- [14] **Ampah, J, D., Yusuf, A, A., Agyekum, E, B., Afrane, S., Jin, C., Liu, H., Fattah, I, M, R., Show, P, L., Shouran, M., Habil, M., Kamel, S.** (2022). Progress and Recent Trends in the Application of Nanoparticles as Low Carbon Fuel Additives—A State of the Art Review. – *MDPI. Nanomaterials*. Volume 12. [on-line] <https://www.mdpi.com/2079-4991/12/9/1515>
(12.07.2023).
- [15] **Zhao, J., Sun, J., Meng, X., Li, Z.** (2022). Recent Advances in Vehicle Exhaust Treatment with Photocatalytic Technology. – *MDPI. Catalysts*. Volume 12. [on-line] <https://www.mdpi.com/2073-4344/12/9/1051> (12.07.2023).
- [16] **Kumar, M, V., Babu, A, V., Reddy, C, R., Pandian, A., Bajaj, M., Zawbaa, H, M., Kamel, S.** (2022). Investigation of the combustion of exhaust gas recirculation in diesel engines with a particulate filter and selective catalytic reactor technologies for environmental gas reduction. – *Elsevier. Case Studies in Thermal Engineering*. Volume 40. [on-line] <https://www.sciencedirect.com/science/article/pii/S2214157X22007948> (12.07.2023).

- [17] LBX H03D – Digital magnetic stirrer with heating – *Labbox*. [on-line] <https://labbox.eu/product/digital-magnetic-stirrer-with-heating-and-ceramic-coated-plate-lbx-h03d-series-3-l/> (15.03.2024).
- [18] OHAUS Frontier FC707 – Multi-Function centrifuge – *Ohaus*. [on-line] <https://mx.ohaus.com/en-us/products/equipment/centrifuges/frontier-5000-series-multi/centrifuge-multi-100-230v-fc5707-r05> (15.03.2024).
- [19] KERN ALJ 200-5DA – Analytical balance – *Kern-Sohn*. [on-line] <https://www.kern-sohn.com/shop/en/products/laboratory-balances/TALJG-220-5-A/> (15.03.2024).
- [20] LBX Ultrasonic cleaner – Mini ultrasonic bath with timer – *Labbox*. [on-line] <https://labbox.eu/product/mini-ultrasonic-bath-with-timer-without-heating-lbx-ultr-small-series/> (15.03.2024).
- [21] VWR UV-1600PC – UV/Visible spectrophotometer – *Vwr*. [on-line] <https://si.vwr.com/store/product/20824776/vwr-uv-1600pc-uv-visible-spectrophotometer> (15.03.2024).
- [22] Memmert UN30 – Laboratory oven – *Memmert*. [on-line] <https://www.memmert.com/products/heating-drying-ovens/universal-oven/UN30/> (15.03.2024).
- [23] ThermoFisher Nicolet iS10 – FTIR spectrometer – *ThermoFisher*. [on-line] <https://www.thermofisher.com/order/catalog/product/IQLAADGAAGFAHDMAPC> (30.04.2024).
- [24] FEI QUANTA 250 – Environmental scanning-electron microscope – *CIC nanoGUNE*. [on-line] <https://www.nanogune.eu/en/nanogune-at-a-glance/facilities-equipment/equipment/environmental-scanning-electron-microscope-esem-fei-quanta-250> (30.04.2024).
- [25] DEWE-43A – Data acquisition system – *DEWESoft*. [on-line] <https://dewesoft.com/products/dewe-43> (22.05.2024).
- [26] Bosch BEA 350 – Emissions analysis – *Bosch*. [on-line] http://www.adesystems.co.uk/brochures/bosch_mot_emissions_bea850_bea350_general.pdf (22.05.2024).
- [27] OriginPro – Data analysis software – *OriginLab*. [on-line] <https://www.originlab.com/index.aspx?go=Products/Origin> (22.05.2024).
- [28] DewesoftX – Data acquisition and digital signal processing software – *DEWESoft*. [on-line] <https://dewesoft.com/products/dewesoftx> (22.05.2024).
- [29] **Kelus, S.** (2023). Transmittance Properties of ZnO Nanorods Used in Solar Cells. – *EMU DSpace*. [on-line] <https://dspace.emu.ee/handle/10492/8488> (01.12.2023).

- [30] **Filatova, E. O., Konashuk, As.** (2015). Interpretation of the Changing the Band Gap of Al₂O₃ Depending on Its Crystalline Form: Connection with Different Local Symmetries. – *ResearchGate. The Journal of Physical Chemistry*. Volume 119. [on-line] https://www.researchgate.net/publication/281643805_Interpretation_of_the_Changing_the_Band_Gap_of_Al2O3_Dependent_on_Its_Crystalline_Form_Connection_with_Different_Local_Symmetries (15.01.2024).
- [31] **Junaid, M., Hussain, S. G., Abbs, N., Khan, W. Q.** (2023). Band gap analysis of zinc oxide for potential bio glucose sensor. – *Elsevier. Results in Chemistry*. Volume 5. [on-line] <https://www.sciencedirect.com/science/article/pii/S221171562300200X> (15.01.2024).
- [32] **Rauwel, E., Galeckas, A., Rauwel, P., Sunding, M. F., Fjellvag, H.,** (2011). Precursor-Dependent Blue-Green Photoluminescence Emission of ZnO Nanoparticles. – *ResearchGate. The Journal of Physical Chemistry*. Volume 115. [on-line] https://www.researchgate.net/publication/235695811_Precursor-Dependent_Blue_Green_Photoluminescence_Emission_of_ZnO_Nanoparticles (15.05.2024).

ÜLDKOKKUVÕTE

Käesoleva magistritöö eesmärk oli uurida nanoosakeste mõju lennukikütusele. Kirjanduse ülevaate põhjal viidi testid läbi rohesünteesi meetodil sünteesitud alumiiniumoksiidi ja tsinkoksiidi nanoosakestega. Rohesünteesi valik oli ajendatud selle keskkonnasõbralikkusest ja varasematest uuringutest. Päevalilleseemned valiti prekursoriks kõrge õlisisalduse tõttu, mis hõlbustas nanoosakeste homogeenset hajumist lennukikütuses, mille tulemuseks on kolloidne lahus.

Kirjanduse ülevaates kajastati erinevaid uuringuid, mis näitavad diislikütuse ja nanoosakeste lisandite katsete positiivseid tulemusi, hõlmates erinevaid nanoosakeste tüüpe ja kontsentratsioone erinevates kütusevariantides. Nanoosakeste sünteesiks valiti alumiiniumoksiid ja tsinkoksiid, kusjuures alumiiniumoksiid valiti sellest tehtud põhjalike uurimistööde tõttu ning tsinkoksiid valiti selle keskkonnasõbralikkuse ja eelnevate laborikatsete tõttu.

Pärast viit sünteesi valiti tsinkoksiid järgmisteks kütuse- ja mootorikatseteks, kuna alumiiniumoksiidil oli tsinkoksiidiga võrreldes kehv saagikus ja esinesid sünteesiprobleemid. Täpsuse tagamiseks viidi läbi mõlema Jet A-1 kütusega füüsikalised ja keemilised testid, mis hõlmasid destilleerimisekarakteristikuid, leekpunkti ja tiheduse analüüsi. Kütuseproovide analüüs näitas mitmeid tähelepanuväärseid tulemusi. Vaatamata samadele tsetaaniindeksi väärtustele, mis näitavad nanoosakeste minimaalset mõju süttimiskvaliteedile, täheldati nanoosakesi sisaldavas proovis leekpunkti olulist vähenemist, mis viitab suurenenud süttivusele. Tiheduse mõõtmised näitasid proovide vahel minimaalset erinevust, mis viitab nanoosakeste lisamisest tulenevale marginaalsele mõjule kütuse tihedusele.

Et hinnata 100 ppm ZnO nanoosakeste mõju Jet A-1 kütuses, mõõdeti mootoritestidega erinevaid parameetreid, sealhulgas õhukiirust, temperatuuri, rõhku ja heitgaaside koostist. Tulemused näitasid, et ZnO nanoosakesed parandasid mootori jõudlust, mida näitavad suurenenud õhukiirused, temperatuurid ja rõhud.

ZnO lisamine tõi aga kaasa suuremad heitkogused: CO suurenes 0,105%-lt 0,112%-le, CO₂ tõusis 2,53%-lt 2,56%-le, süsivesinike hulk kasvas 34 ppm-lt 49 ppm-ni (kasv 44,1%) ja NO_x-emissioon tõusis 10 ppm kuni 12 ppm (kasv 20%). Suurenenud NO_x heitkogused on

tõenäoliselt tingitud NO_3 molekulide olemasolust sünteesiks kasutatud tsingi prekursorist, mida on täheldatud FTIR analüüsidest. Nanoosakeste täiendav loputamine võib potentsiaalselt vähendada HC heitkoguseid, eemaldades sünteesi jääkproduktid.

Mootoritestide tulemused ei ühti kirjanduses tavaliselt esitatud tulemustega. Varasemate uuringute kohaselt on ZnO nanoosakeste lisamine kütuse koostisesse sageli seotud saasteainete, nagu CO, HC ja NO_x , heitkoguste vähenemisega. See lahknevus viitab sellele, et ZnO nanoosakeste mõju põlemisprotsessidele võib varieeruda sõltuvalt konkreetsest mootori konfiguratsioonist, töötingimustest ja kütuse koostisest. Täiendav uurimine on vajalik, et mõista täheldatud heitkoguste suurenemise eest vastutavaid mehhanisme.

Kokkuvõtteks võib öelda, et kuigi 100 ppm ZnO lisamine Jet A-1 kütusele suurendab mootori jõudlust, põhjustab see ka suuremaid saasteainete heitkoguseid, mistõttu on vaja hoolikalt kaaluda selle keskkonnamõju ja võimalikke meetmeid nende heitmete vähendamiseks. Rohkem on vaja uurida ZnO nanoosakeste sünteesi ning Jet A-1 ja nanoosakeste stabiilsete kolloidsete lahuste loomist, mis püsivad stabiilsena pikema aja jooksul. Selle stabiilsuse saavutamiseks tuleks uurida nanoosakeste katmise ja jahvatamise täiustatud tehnikaid. Lisaks tuleks selle uurimistöö tulemusi kinnitada täiendavate kütuse- ja mootorikatsetega ning katsetada nanoosakeste lisandite erinevaid kontsentratsioone, et optimeerida jõudlust ja heitkoguseid. Nanoosakeste kütusefiltrile avaldatava mõju uurimine on samuti oluline, et tagada nende lisandite pikaajaline elujõulisus praktilistes rakendustes.

APPENDIXES

Appendix A. Lihtlitsents lõputöö salvestamiseks ja üldsusele kättesaadavaks tegemiseks ning juhendajate kinnitus lõputöö kaitsmisele lubamise kohta

Mina, Richard Erelt,

sünniaeg 19.09.1999,

1. annan Eesti Maaülikoolile tasuta loa (lihtlitsentsi) enda koostatud lõputöö
Assessment of Nanoparticles-Based Additives in Jet-Fuels Combustion,

mille juhendaja(d) on Erwan Yann Rauwel, Siim Küünal, Karl-Eerik Unt,

1.1. salvestamiseks säilitamise eesmärgil,

1.2. digiarhiivi DSpace lisamiseks ja

1.3. veebikeskkonnas üldsusele kättesaadavaks tegemiseks
kuni autoriõiguse kehtivuse tähtaja lõppemiseni;

2. olen teadlik, et punktis 1 nimetatud õigused jäävad alles ka autorile;

3. kinnitan, et lihtlitsentsi andmisega ei rikuta teiste isikute intellektuaalomandi ega
isikuandmete kaitse seadusest tulenevaid õigusi.

Lõputöö autor

Richard Erelt
(allkirjastatud digitaalselt)

Tartu, (kuupäev digiümbrikus)

Juhendaja(te) kinnitus lõputöö kaitsmisele lubamise kohta

Luban lõputöö kaitsmisele.

Erwan Yann Rauwel
(allkirjastatud digitaalselt)

(kuupäev digiümbrikus)

Siim Küünal
(allkirjastatud digitaalselt)

(kuupäev digiümbrikus)

Karl-Eerik Unt
(allkirjastatud digitaalselt)

(kuupäev digiümbrikus)